J Elast (2011) 105:137–170
DOI 10.1007/s10659-010-9290-5

Wrinkling of a Stretched Thin Sheet

Eric Puntel · Luca Deseri · Eliot Fried

Received: 8 October 2010 / Published online: 23 December 2010

Abstract When a thin rectangular sheet is clamped along two opposing edges and stretched, its inability to accommodate the Poisson contraction near the clamps may lead to the formation of wrinkles with crests and troughs parallel to the axis of stretch. A variational model for this phenomenon is proposed. The relevant energy functional includes bending and membranal contributions, the latter depending explicitly on the applied stretch. Motivated by work of Cerda, Ravi-Chandar, and Mahadevan, the functional is minimized subject to a global kinematical constraint on the area of the mid-surface of the sheet. Analysis of a boundary-value problem for the ensuing Euler–Lagrange equation shows that wrinkled solutions exist only above a threshold of the applied stretch. A sequence of critical values of the applied stretch, each element of which corresponds to a discrete number of wrinkles, is determined. Whenever the applied stretch is sufficiently large to induce more than three wrinkles, previously proposed scaling relations for the wrinkle wavelength and, modulo a multiplicative factor that depends on the Poisson ratio of the sheet and the applied stretch and arises from the more general and weaker nature of geometric constraint under consideration, root-mean-square amplitude are confirmed. In contrast to the scaling relations for the wrinkle wavelength and amplitude, the applied stretch required to induce any number of wrinkles depends on the in-plane aspect ratio of the sheet. When the sheet is significantly longer than it is wide, the critical stretch scales with the fourth power of the length-to-width

Dedicated to the memory of Donald E. Carlson, whose insight and clarity of thought were exceeded only by his modesty and generosity.

E. Puntel
Dipartimento di Georisorse e Territorio, Università di Udine, via Cotonificio 114, 33100 Udine, Italy

L. Deseri
Dipartimento di Ingegneria Meccanica e Strutturale, Università di Trento, via Mesiano 77, 38023 Trento, Italy

E. Fried (✉)
Department of Mechanical Engineering, McGill University, 817 Sherbrooke Street West, Montréal, Québec H3A 2K6, Canada
e-mail: eliot.fried@mcgill.ca

ratio but, when the sheet is significantly wider than it is long, the critical stretch scales with the square of that same ratio.

Keywords Föppl–von Kármán theory · Thin film · Wrinkling · Buckling · Critical load

Mathematics Subject Classification (2000) 74K35 · 74G60

1 Introduction

A membrane subject to in-plane loading involving a combination of shear and tension will generally exhibit taut, wrinkled, and slack zones. In taut zones, the in-plane principal stresses are tensile. In wrinkled zones, one of the in-plane stresses vanishes and the crests and troughs of the wrinkles are roughly parallel to trajectories of nonvanishing tension. In slack zones, which do not appear in the absence of wrinkles, the in-plane principal stresses both vanish.

Wrinkles can be viewed as manifestations of an instability arising from the almost negligible flexural stiffness of membranes and the associated inability to withstand compressive loading. From an energetic perspective, experimental observations indicate that, at least for certain loading configurations and magnitudes, the work needed to deform a membrane elastically without producing wrinkles may be more costly than otherwise. Moreover, because wrinkles form along lines of maximum tensile load, load carrying capacity is increased along those lines.

Wrinkles can adversely affect the performance and longevity of membrane structures. Blandino, Johnson and Dharamsi [1] note that this is currently of particular importance for expandable and inflatable thin-film membrane structures such as tubular booms, telescopic masts, solar sails, solar panels, and reflector antennas for applications in space. Obvious advantages of such structures are that they are lightweight and can be compactly stowed. However, such structures must often meet stringent surface tolerances over very large areas. For example, Jenkins, Kalanovic, Padmanabhan and Faisal [2] show that allowable wavefront errors for reflector antennas should not exceed five percent of the wavelength of interest.

For standard applications involving structural membranes, the traditional approach to avoiding wrinkles is to introduce compensating supports such as pillars and arches and attach cables to the edges and interior of the membrane, all with the goal of applying tension as uniformly as possible throughout the membrane surface. As Sakamoto, Park and Miyazaki [3] observe, this approach involves unavoidable weight increases. Moreover, large tensile stresses can increase risks of material creep, crack initiation and propagation, and failure. For applications of membrane structures in space, there seems to be little choice but to develop the capability to reliably estimate and control, if not completely suppress, wrinkles.

Such capability is likely to be valuable in various other areas of current importance. In the medical field, there is a need for wound and burn treatments (Hudson and Renshaw [4]) and for surgical techniques that ensure proper circulation, mobility, and minimal scarring subsequent to healing (Lott-Crumpler and Chaudhry [5], Georgeu and Ross [6], Cerda [7], Hofer and Mureau [8], Ueda, Hara, Okada, Kurokawa, Otani and Nuri [9]). Optical measurements of wrinkles on thin polymer films might provide a simple and accurate alternative to more traditional techniques used to determine thicknesses, mechanical properties (Stafford, Harrison, Beers, Karim, Amis, Vanlandingham, Kim, Volksen, Miller and Simonyi [10]), and residual stresses (Chung, Chastek, Fasolka, Ro and Stafford [11]). Similarly, measuring wrinkles on cell membranes might provide important insight regarding cell locomotion (Burton and Taylor [12], Harris, Wild and Stopak [13]). Applications that exploit wrinkling

to tune the optical properties of cavities (Kolaric, Vandeparre, Desprez, Vallee and Damman [14]) and to shape capillaries for micro-fluidic purposes (Ohzono, Monobe, Shiokawa, Fujiwara and Shimizu [15]) also seem relevant.

Interest in modeling wrinkle formation appears to go back at least as far as a five-part paper published in 1929 by Wagner [16], whose concern was with structural elements like thin beam webs and wing spars carrying loads in excess of those required to induce buckling. Wagner's strategy was to treat such elements as linearly elastic plates and assume that out-of-plane flexural and in-plane compressive stresses are negligible relative to in-plane tensile stresses. These stipulations form the basis of tension-field theory, as developed further by Wagner and Ballerstedt [17], Wagner [18], Kondo [19], Reissner [20], Mansfield [21], Danielson and Natarajan [22], Wu [23], Zac [24], Pipkin [25], Steigmann and Pipkin [26], and Steigmann [27].

Mansfield [21] used variational arguments to show that lines of tension in a wrinkled membrane coincide with trajectories along which the strain energy of the membrane is maximized. Kondo [19] and Zac [24] deduced that these trajectories correspond to geodesics on the surface of the deformed membrane (a particularly elegant proof of this result is given by Steigmann [27]). With a view to modeling skin, polymers, and textiles, Danielson and Natarajan [22] and Wu [23] accounted for geometric and constitutive nonlinearities.

Solutions to boundary-value problems arising from tension-field theory do not provide information about the wavelengths and amplitudes of wrinkles. Instead, these solutions involve infinitely many wrinkles, each of infinitesimal amplitude, spaced infinitesimally close together. Pipkin [25], Steigmann and Pipkin [26], and Steigmann [27] developed a minimum-energy principle that delivers the central tenets of tension-field theories as results rather than postulates and accounts for geometric and material nonlinearities. The energy functionals governed by this principle are generally nonconvex and, thus, do not possess unique minimizers. Pipkin [25], Steigmann and Pipkin [26] and Steigmann [27] showed that relaxed energy functionals have unique minimizers. However, consistent with well-known properties of solutions to boundary-value problems of tension-field theory, these minimizers involve infinitesimally-fine distributions of wrinkles.

In an actual membrane, the small bending stiffness that tension-field theory neglects sets a finite lower limit to the wavelength of wrinkles. Information concerning the distribution of stresses and the overall locations of wrinkled and slack zones suffice in many conventional applications. However, applications where tolerances for optical precision must be met or where measurements of the wavelengths and amplitudes of wrinkles are needed to determine geometric or constitutive properties require knowledge of the detailed distributions of wrinkles.

The above mentioned applications and the limitations of tension-field theory are indicative of the need for approaches that account for both membranal and bending contributions to the free energy. Several proposals are available in the literature, including an early one by Hilgers and Pipkin [28] and a more recent one by Steigmann [29]. Here, however, we are guided by papers of Cerda, Ravi-Chandar and Mahadevan [30] and Cerda & Mahadevan [31], whose work can be regarded as seminal for both its novelty and its contribution to reawakened interest in wrinkling.

In stretching experiments performed on rectangular polyethylene sheets, Cerda, Ravi-Chandar and Mahadevan [30] found that compressive stresses leading to wrinkles parallel to the direction of stretching arise due to the inability of the specimen to accommodate the Poisson contraction near clamped edges. To explain this observation, Cerda, Ravi-Chandar and Mahadevan [30] and, in somewhat more detail, Cerda and Mahadevan [31] considered

the variational problem of extremizing an energy functional $\mathcal{U}$ of the form

$$\mathcal{U} = \mathcal{F}^{\mathrm{b}} + \mathcal{F}^{\mathrm{m}} - \varepsilon^* \mathcal{T},$$

where $\mathcal{F}^{\mathrm{b}}$ is the bending energy, $\mathcal{F}^{\mathrm{m}}$ is the membranal energy, and $\varepsilon^*\mathcal{T}$ is a penalty term that enforces a constraint imposed to ensure that the membrane is inextensible in the direction of wrinkling. Taking into account various simplifying assumptions, Cerda, Ravi-Chandar and Mahadevan [30] and Cerda and Mahadevan [31] observe that the combination $\mathcal{F}^{\mathrm{b}} + \mathcal{F}^{\mathrm{m}}$ of bending and stretching terms falls within the general framework of the Föppl–von Kármán theory of plates. The penalty term is new and its presence allows for the determination of scaling relations for not only the wavelength λ but also the amplitude A of wrinkles. For a sheet of length $2L_1$, width $2L_2$, thickness h, and Poisson's ratio ν stretched by an amount ε, λ and A scale with the $1/2$ power of the product $L_1 h$. Further, λ scales with the $-1/4$ power of both ε and $(1-\nu^2)$ and A scales with the $1/4$ power of ε and $\nu^2/(1-\nu^2)$.

In studies of sheets subject to boundary conditions involving radial axisymmetric stretch (Coman [32]) and in-plane shears (Wong and Pellegrino [33]), derived scaling relations that, modulo geometric prefactors, are identical to those of Cerda, Ravi-Chandar and Mahadevan [30] and Cerda and Mahadevan [31]. This supports the view that the scaling relations for wrinkle wavelengths and amplitudes might be rather insensitive to boundary conditions and, in this sense, universal.

The work presented here was first stimulated by the aim to determine the critical stretch at the onset of wrinkling, information that was not provided in previous work. This formulation and analysis needed to achieve this aim are somewhat more elaborate than those of Cerda and Mahadevan [31]. Although the analysis rests on a constrained Föppl–von Kármán model, several features of the model differ from that considered by Cerda, Ravi-Chandar and Mahadevan [30] and Cerda and Mahadevan [31]. In-plane stretching is accounted for by an imposed prestrain and the stretching energy $\mathcal{F}^{\mathrm{m}}$ accounts for three-dimensional energetic contributions both parallel and perpendicular to the axis of the applied stretch. Moreover, the constraint is weaker than that used by Cerda and Mahadevan [31] and allows for dependence upon the Poisson ratio of the sheet and the applied stretch. Another distinguishing feature of the formulation is the lack of any a priori assumption on the shape of the wrinkle profile in the direction orthogonal to the imposed prestrain.

A careful analysis of the equilibrium conditions shows that not one but two wavelengths arise. Of these, one can be identified as the actual wrinkle wavelength. The other is approximately equal to twice the sheet width and wraps the cross-width wrinkle profile in a half-sine shape with maximum amplitude at half width and minimum amplitude at the free edges. Notably, it is found that the scaling relation for the wavelength λ of wrinkling derived by Cerda, Ravi-Chandar and Mahadevan [30] and Cerda and Mahadevan [31] remains valid whenever the stretch ε applied to the sheet is sufficiently large relative to a reference stretch $\bar{\varepsilon}$ determined in terms of the length $2L_1$, thickness h, and Poisson's ratio ν of the sheet by $\bar{\varepsilon} = \pi^2 h^2/48 L_1^2 (1-\nu^2)$.

Granted that the applied stretch ε is sufficiently large relative to $\bar{\varepsilon}$, the analysis also yields a scaling relation for the root-mean-square of the wrinkle amplitudes. That relation is consistent, but for one prefactor, with the analogous relation obtained by Cerda, Ravi-Chandar and Mahadevan [30] and Cerda and Mahadevan [31], who assume a constant wrinkle amplitude. The factor of discrepancy, which involves Poisson's ratio and the applied stretch, reflects the influence of the geometric constraint on the wrinkle amplitude. A particular specialization of the constraint used here reduces this factor to unity and, thus, allows the recovery of the

scaling relation obtained by Cerda, Ravi-Chandar and Mahadevan [30] and Cerda and Mahadevan [31]. However, in general, the presence of this factor permits an investigation of broader classes of constraints consistent with experimental observations.

Most importantly, the analysis presented here yields an explicit relation for a sequence of critical applied stretches associated with the formation of different numbers of wrinkles. The transition from a state involving $n > 0$ wrinkles to a state involving $n + 1$ wrinkles is found to be abrupt and discontinuous. Wong and Pellegrino [34, 35] observed jumps consistent with this result in experiments on shear-induced wrinkling, as did Balmforth, Craster, and Slim [36] in numerical simulations of wrinkling induced by an imposed shear or by a body force such as gravity.

For the case of a stretched sheet, the results obtained here suggest the need for experiments designed to measure wrinkle amplitudes and critical applied stretches and to explore the validity of various geometric constraints.

2 Preliminaries

Consider a rectangular sheet of length $2L_1$, width $2L_2$, and thickness h. Choose a positively-oriented, orthonormal basis $\{\mathbf{e}_1, \mathbf{e}_2, \mathbf{e}_3\}$ with associated Cartesian coordinates x_1, x_2, and x_3 such that

$$-L_1 \le x_1 \le L_1, \quad -L_2 \le x_2 \le L_2, \quad -\frac{1}{2}h \le x_3 \le \frac{1}{2}h. \tag{1}$$

Motivated by the experiments of Cerda, Ravi-Chandar & Mahadevan [30], suppose that the $x_1 = \pm L_1$ edges of the sheet are pinned and subject to uniform displacements

$$\mathbf{u}(\pm L_1, x_2, x_3) = \pm \varepsilon L_1 \mathbf{e}_1, \qquad -L_2 \le x_2 \le L_2, \quad -\frac{1}{2}h \le x_3 \le \frac{1}{2}h, \tag{2}$$

with $\varepsilon > 0$. Away from these edges, the homogeneous displacement field $\bar{\mathbf{u}}$ satisfying

$$\bar{\mathbf{u}}(x_1, x_2, x_3) = \varepsilon x_1 \mathbf{e}_1 - \nu \varepsilon (x_2 \mathbf{e}_2 + x_3 \mathbf{e}_3), \tag{3}$$

is admissible in the sense that it satisfies the Cauchy–Navier equations of three-dimensional isotropic elastostatics and satisfies the traction-free boundary conditions on the free edges and surfaces. However, in the experiments of Cerda, Ravi-Chandar & Mahadevan [30], the applied stretch ε produces deformations which exhibit out-of-plane wrinkles along the $\mathbf{e}_2$-direction. To accommodate this observation as simply as possible, while allowing for potential inhomogeneity induced by the boundary conditions, consider a modification $\mathbf{u}$ of $\bar{\mathbf{u}}$ defined so that:[1]

$$\mathbf{u}(x_1, x_2, x_3) = \bar{\mathbf{u}}(x_1, x_2, x_3) + w(x_1, x_2)\mathbf{e}_3. \tag{4}$$

The Green–St. Venant strain-tensor $\mathbf{D} = \frac{1}{2}(\nabla \mathbf{u} + (\nabla \mathbf{u})^\top + (\nabla \mathbf{u})^\top \nabla \mathbf{u})$ corresponding to the particular choice (4) of $\mathbf{u}$ is given by[2]

$$\mathbf{D} = \bar{\mathbf{E}} + \frac{1}{2}\bar{\mathbf{E}}^2 + \frac{1}{2}(1 - \nu)(\mathbf{e}_3 \otimes \mathbf{e}_\alpha + \mathbf{e}_\alpha \otimes \mathbf{e}_3) + \frac{1}{2} w_{,\alpha}\, w_{,\beta}\, \mathbf{e}_\alpha \otimes \mathbf{e}_\beta \tag{5}$$

[1] The Kirchhoff–Love term $x_3 w_{,\alpha}\, \mathbf{e}_\alpha$, which is absent from (4), contributes to the bending energy discussed subsequently.

[2] Throughout this paper, subscripts involving Greek characters range over $\{1, 2\}$, $w_{,\alpha}$ denotes the partial derivative of w with respect to x_α, and the usual summation convention is employed.

where

$$\bar{\mathbf{E}} = \varepsilon[\mathbf{e}_1 \otimes \mathbf{e}_1 - \nu(\mathbf{e}_2 \otimes \mathbf{e}_2 + \mathbf{e}_3 \otimes \mathbf{e}_3)]. \tag{6}$$

is the homogeneous prestretch associated with the homogenous displacement field defined in (3). For problems involving thin sheets with nonnegligible deflections, it is common (Landau & Lifschitz [37]) to replace the full expression (5) for the Green–St. Venant strain-tensor by the Föppl–von Kármán approximation

$$\mathbf{E} = \bar{\mathbf{E}} + \frac{1}{2} w_{,\alpha} w_{,\beta} \mathbf{e}_\alpha \otimes \mathbf{e}_\beta. \tag{7}$$

Assumptions sufficient to ensure that $\mathbf{E}$ approximates $\mathbf{D}$ accurately, such as those stated in detail by Bažant & Cedolin [38, pp. 713–714], are hereafter assumed to hold and $\mathbf{E}$ as defined by (7) is adopted as the relevant membranal strain measure.

3 Free Energy of the Sheet

Model the sheet as linearly elastic and isotropic with given Young's modulus E and Poisson's ratio ν consistent with the classical inequalities

$$E > 0 \quad \text{and} \quad -1 < \nu < 1/2. \tag{8}$$

Motivated by the discussion leading to the truncated form $\mathbf{E}$ of the Green–St. Venant strain-tensor $\mathbf{D}$, assume that the free energy of the sheet is given by a sum,

$$\mathcal{F} = \mathcal{F}^{\mathrm{b}} + \mathcal{F}^{\mathrm{m}}, \tag{9}$$

of a classical bending contribution

$$\mathcal{F}^{\mathrm{b}} = \frac{Eh^3}{24(1-\nu^2)} \int_{-L_1}^{L_1} \int_{-L_2}^{L_2} \left[w_{,\alpha\alpha}\, w_{,\beta\beta} - (1-\nu)(w_{,\alpha\alpha}\, w_{,\beta\beta} - w_{,\alpha\beta}\, w_{,\alpha\beta}) \right] \mathrm{d}x_2\, \mathrm{d}x_1 \tag{10}$$

and a membranal contribution

$$\mathcal{F}^{\mathrm{m}} = \int_{-L_1}^{L_1} \int_{-L_2}^{L_2} \int_{-h/2}^{h/2} \frac{1}{2} \mathbf{T} \cdot \mathbf{E}\, \mathrm{d}x_3\, \mathrm{d}x_2\, \mathrm{d}x_1, \tag{11}$$

with the stress $\mathbf{T}$ determined in accord with

$$\mathbf{T} = \bar{\mathbf{T}} + \frac{E}{2(1+\nu)} \left(w_{,\alpha}\, w_{,\beta}\, \mathbf{e}_\alpha \otimes \mathbf{e}_\beta + \frac{\nu}{1-2\nu} w_{,\alpha}\, w_{,\alpha}\, \mathbf{e}_i \otimes \mathbf{e}_i \right), \tag{12}$$

where

$$\bar{\mathbf{T}} = E\varepsilon \mathbf{e}_1 \otimes \mathbf{e}_1 \tag{13}$$

is the uniaxial stress associated with the homogeneous displacement field $\bar{\mathbf{u}}$ defined in (3).

In view of (7) and (12), the energy density $\mathbf{T} \cdot \mathbf{E}$ is given by

$$\mathbf{T} \cdot \mathbf{E} = E(\varepsilon^2 + \varepsilon w_{,1}^2) + \frac{E(1-\nu)}{4(1+\nu)(1-2\nu)} (w_{,\alpha}\, w_{,\alpha})^2, \tag{14}$$

which, in addition to the classical term proportional to $(w_{,\alpha}\, w_{,\alpha})^2$, includes two terms arising from the imposed stretch ε. Whereas the term $E\varepsilon^2$ delivers the constant, and therefore inconsequential, free energy associated with the homogeneous displacement field $\bar{\mathbf{u}}$, the term $\varepsilon w_{,1}^2$ penalizes deflection along the axis $\mathbf{e}_1$ of the applied stretch.

By (14), $\mathbf{T}\cdot\mathbf{E}$ is independent of the through-thickness coordinate x_3 and the definition (11) of the membranal free-energy reduces to

$$\mathcal{F}^{\mathrm{m}} = \frac{Eh}{2}\int_{-L_1}^{L_1}\int_{-L_2}^{L_2}\left(\varepsilon^2 + \varepsilon w_{,1}^2 + \frac{1-\nu}{4(1+\nu)(1-2\nu)}(w_{,\alpha}\, w_{,\alpha})^2\right)\mathrm{d}x_2\,\mathrm{d}x_1. \tag{15}$$

An interesting alternative to (15) which exhibits the energetic impact of deflections perpendicular to the axis of the applied stretch follows on introducing

$$a = \frac{(1+\nu)(1-2\nu)}{1-\nu}, \tag{16}$$

noting that

$$\begin{aligned}\mathbf{T}\cdot\mathbf{E} &= E(\varepsilon^2 + \varepsilon w_{,1}^2) + \frac{E}{4a}(w_{,\alpha}\, w_{,\alpha})^2\\ &= \frac{E}{a}\left[\left(a\varepsilon + \frac{1}{2}w_{,\alpha}\, w_{,\alpha}\right)^2 - a\varepsilon w_{,2}^2\right] + (1-a)\varepsilon^2\\ &= \frac{E(1-\nu)}{(1+\nu)(1-2\nu)}\left[\left(a\varepsilon + \frac{1}{2}w_{,\alpha}\, w_{,\alpha}\right)^2 - a\varepsilon w_{,2}^2\right] + \frac{2E\nu^2\varepsilon^2}{1-\nu}\end{aligned} \tag{17}$$

and bearing in mind that the free energy can be determined only up to an additive, normalizing, constant (so that the constant contribution $2\nu^2\varepsilon^2/(1-\nu)$ to the membranal free-energy $\mathcal{F}^{\mathrm{m}}$ can be neglected without loss of generality), it follows from (11), (14), and (16) that

$$\mathcal{F}^{\mathrm{m}} = \frac{Eh(1-\nu)}{2(1+\nu)(1-2\nu)}\int_{-L_1}^{L_1}\int_{-L_2}^{L_2}\left[\left(a\varepsilon + \frac{1}{2}w_{,\alpha}\, w_{,\alpha}\right)^2 - a\varepsilon w_{,2}^2\right]\mathrm{d}x_2\,\mathrm{d}x_1. \tag{18}$$

4 Geometrical Constraint

Cerda & Mahadevan [31] describe the stretching experiments of Cerda, Ravi-Chandar & Mahadevan [30] with a Föppl–von Kármán type model for the bending and stretching of the sheet augmented by the constraint

$$\int_{-L_2}^{L_2}\left(\sqrt{1+w_{,2}^2} - 1\right)\mathrm{d}x_2 = \delta, \tag{19}$$

where δ is a prescribed scalar displacement along the $\mathbf{e}_2$-direction. To account for the observed inhomogeneous transverse shrinking of the sheet, Cerda & Mahadevan [31] state that δ may vary with x_1 but eventually take it to be a constant proportional to $\nu\varepsilon$, with ε being the applied stretch introduced in (2). Cerda & Mahadevan [31] justify the imposition of (19) on the grounds that the sheet should be inextensible in the $\mathbf{e}_2$-direction. Without (19), Cerda & Mahadevan [31] would not be able to determine a relation for the wrinkle amplitude.

Here, a constraint somewhat weaker than (19) is imposed. This constraint requires that

$$\frac{1}{4L_1L_2}\int_{-L_1}^{L_1}\int_{-L_2}^{L_2}\left(\sqrt{1+w_{,\alpha}\,w_{,\alpha}}-1\right)\mathrm{d}x_2\,\mathrm{d}x_1=\varepsilon g(\nu,\varepsilon), \tag{20}$$

where g must be nonnegative for all relevant values of ν and all sufficiently small values of ε:

$$g(\nu,\varepsilon)>0, \qquad -1<\nu<\frac{1}{2}, \qquad 0<\varepsilon\ll 1. \tag{21}$$

The integral on the left side of (20) measures the extent to which wrinkling changes the surface area of the midplane of the sheet. For materials such as polymeric solids for which $\nu>0$, $(21)_1$ ensures that wrinkling is accompanied by an area increase. It will be shown that, to leading-order terms in the ratio h/L_1, choosing $g(\nu,\varepsilon)=\nu$ in (20) yields a scaling relation for the root-mean-square of the wrinkle amplitudes that is consistent with the result obtained by Cerda, Ravi-Chandar and Mahadevan [30] and Cerda & Mahadevan [31].

The constraints (19) and (20) raise some concern. In contrast to being local, pointwise constraints of the variety classically encountered in continuum mechanics,[3] (19) and (20) are global and a fundamental basis for such constraints is currently lacking. Another delicate issue that deserves consideration but is not pursued here concerns material symmetry. Generally, a constraint should be invariant under the same symmetry transformations of the underlying material.[4] In this respect, (20)—which is insensitive to in-plane rotations of the gradient of w and, thus, is consistent with the assumption that the sheet is transversely isotropic—appears preferable to (19). However, (20) is not consistent with the isotropy of the membranal stress $\mathbf{T}$ defined in (12).

5 Net Potential-Energy of the System. Euler–Lagrange Equation

The net potential-energy $\mathcal{U}$ of the system is given by

$$\mathcal{U}=\mathcal{F}^{\mathrm{b}}+\mathcal{F}^{\mathrm{m}}-\varepsilon^{*}\mathcal{T}, \tag{22}$$

where the bending and membranal contributions $\mathcal{F}^{\mathrm{b}}$ and $\mathcal{F}^{\mathrm{m}}$ are defined by (10) and (18),

$$\mathcal{T}=Eh\int_{-L_1}^{L_1}\int_{-L_2}^{L_2}\left(\sqrt{1+w_{,\alpha}\,w_{,\alpha}}-1-\varepsilon g(\nu,\varepsilon)\right)\mathrm{d}x_2\,\mathrm{d}x_1 \tag{23}$$

is the magnitude of the reactive force, per unit thickness of the sheet, necessary to ensure satisfaction of the constraint (20), and ε^{*} is a (constant) Lagrange multiplier.

The Euler–Lagrange equation corresponding to the potential-energy functional (22) has the form

$$\frac{Eh^3}{12(1-\nu^2)}w_{,\alpha\alpha\beta\beta}-\frac{Eh}{2a}(w_{,\beta}\,w_{,\beta}\,w_{,\alpha})_{,\alpha}-Eh\varepsilon w_{,11}+Eh\varepsilon^{*}\left(\frac{w_{,\alpha}}{\sqrt{1+w_{,\beta}\,w_{,\beta}}}\right)_{,\alpha}=0. \tag{24}$$

[3] See Podio-Guidugli [39] for a lucid perspective on the role of constraints in elasticity theory. See Pipkin [40] for an example of the application of a pointwise constraint to a thin structure.

[4] See Podio-Guidugli [39].

This equation is to be solved on the rectangular domain $(-L_1, L_1) \times (-L_2, L_2)$ corresponding to the mid-plane of the undistorted sheet.

6 Boundary Conditions

In the experiments of Cerda, Ravi-Chandar & Mahadevan [30], the pinned edges of the sheet are displaced consistent with (2), while the faces and remaining edges are traction-free. On the other hand, the fourth-order terms $w_{,\alpha\alpha\beta\beta}$ in the Euler–Lagrange equation (24), require two boundary conditions on each edge of the rectangle $(-L_1, L_1) \times (-L_2, L_2)$.

Consider the pinned edges $x_1 = \pm L_1$ of the sheet. Using (2) and (3) in (4) yields simple conditions

$$w(\pm L_1, x_2) = 0, \quad -L_2 \le x_2 \le L_2, \tag{25}$$

requiring that the deflection vanish. Moreover, since pins accommodate rotations but not bending moments, the condition (25) is augmented by

$$\frac{Eh^3}{12(1-\nu^2)} w_{,11}(\pm L_1, x_2) = 0, \quad -L_2 \le x_2 \le L_2. \tag{26}$$

Consider, next, the remaining edges $x_2 = \pm L_2$ of the sheet. In view of the absence of applied tractions in the experiment of Cerda, Ravi-Chandar & Mahadevan [30], it might seem reasonable to require that the bending moments and the shears vanish at $x_2 = \pm L_2$. However, phenomenologically, the experimental results suggest that the rotations and the normal curvature are negligible along the unpinned edges of the sheet, so that

$$w_{,2}(x_1, \pm L_2) = w_{,22}(x_1, \pm L_2) = 0, \quad -L_1 \le x_1 \le L_1. \tag{27}$$

7 Linearization Based on the Small-Slope Approximation

Invoking the classical small-slope approximation,

$$\sqrt{w_{,\alpha}\, w_{,\alpha}} \ll 1, \tag{28}$$

to linearize the Euler–Lagrange equation (24) gives

$$\frac{Eh^3}{12(1-\nu^2)} w_{,\alpha\alpha\beta\beta} - Eh(\varepsilon - \varepsilon^*) w_{,11} + Eh\varepsilon^* w_{,22} = 0. \tag{29}$$

In view of (25)–(27), the partial-differential equation (29) is to be solved on $(-L_1, L_1) \times (-L_2, L_2)$ subject to the boundary conditions

$$\left.\begin{aligned} w(\pm L_1, x_2) = w_{,11}(\pm L_1, x_2) = 0, \quad & -L_2 \le x_2 \le L_2, \\ w_{,2}(x_1, \pm L_2) = w_{,22}(x_1, \pm L_2) = 0, \quad & -L_1 \le x_1 \le L_1. \end{aligned}\right\} \tag{30}$$

8 Governing Boundary-Value Problem

Consistent with the boundary conditions $(30)_1$ on the pinned ends of the sheet, seek a solution of the partial-differential equation (29) of the form

$$w(x_1, x_2) = \cos\left(\frac{\pi x_1}{2L_1}\right) y(x_2), \tag{31}$$

with y to be determined. Inserting (31) into the partial-differential equation (29) and boundary conditions $(30)_2$ yields a boundary-value problem for y consisting of the ordinary-differential equation

$$B y_{,2222} + P y_{,22} + K y = 0, \tag{32}$$

to be satisfied on $(-L_2, L_2)$, and the boundary conditions

$$y_{,2}(\pm L_2) = y_{,22}(\pm L_2) = 0, \tag{33}$$

where B, P, and K are defined by

$$B = \frac{Eh^3}{12(1-\nu^2)}, \qquad P = \frac{\pi^2 B(\varepsilon^* - 2\bar{\varepsilon})}{4L_1^2\bar{\varepsilon}}, \qquad K = \frac{\pi^4 B(\varepsilon - \varepsilon^* + \bar{\varepsilon})}{16L_1^4\bar{\varepsilon}}, \tag{34}$$

with

$$\bar{\varepsilon} = \frac{\pi^2 B}{4EhL_1^2} = \frac{\pi^2 h^2}{48L_1^2(1-\nu^2)}. \tag{35}$$

In view of (8), B must be positive. Granted that K is also positive, the ordinary differential equation (32) is identical to that governing the buckling of a beam of bending rigidity B (which is the classical reduced bending rigidity of a plate with Young's modulus E, Poisson's ratio ν, and thickness h) bonded perfectly to an elastic foundation with stiffness K and subjected to a load P. This analogy was recognized previously by Cerda & Mahadevan [31], although the specific expressions for the counterparts of the coefficients P and K arising in their work differ from $(34)_{2,3}$.

Here, B, P, and K are referred to as the effective bending rigidity, the effective load, and the stiffness of the effective elastic foundation. Granted, again, that the stiffness K of the effective elastic foundation is positive, oscillatory solutions of the boundary value problem (32)–(33) are to be expected only for compressive values of the effective load P. Consistent with an objective of describing wrinkled states, suppose that P is non negative and K is strictly positive:

$$P \geq 0, \qquad K > 0. \tag{36}$$

In combination with $(34)_{2,3}$, the inequalities (36) imply that the Lagrange multiplier ε^* must be bounded according to

$$2\bar{\varepsilon} \leq \varepsilon^* < \bar{\varepsilon} + \varepsilon. \tag{37}$$

As a consequence of (37), wrinkling is impossible unless the applied stretch ε obeys

$$\varepsilon > \bar{\varepsilon}. \tag{38}$$

Importantly, granted that the effective load and the stiffness of the effective elastic foundation obey (36), (38) is necessary but not sufficient to ensure that the boundary-value problem (32)–(33) possesses a solution with oscillations and, thus, that wrinkling occurs.

From $(34)_2$ and $(34)_3$, the effective compressive load P and the stiffness K of the effective elastic foundation depend on the Lagrange multiplier ε^* and thus, ostensibly, on the applied stretch ε. This stands in contrast to classical problems involving beams on elastic foundations because the parameters P and K entering the boundary-value problem (32) are generally independent in such problems.

9 Nondimensionalization

Define dimensionless independent and dependent variables η and f by

$$\eta = \frac{\pi x_2}{2L_2} \quad \text{and} \quad f(\eta) = \frac{y(x_2)}{2L_2}. \tag{39}$$

Further, define dimensionless versions p and k of the effective compressive load and the stiffness of the effective elastic foundation by

$$p = \frac{4L_2^2 P}{\pi^2 B} \quad \text{and} \quad k = \frac{16L_2^4 K}{\pi^4 B} \tag{40}$$

Then, the ordinary-differential equation (32) and boundary conditions (33) yield

$$f'''' + pf'' + kf = 0 \tag{41}$$

and

$$f'\left(\pm\frac{\pi}{2}\right) = f''\left(\pm\frac{\pi}{2}\right) = 0, \tag{42}$$

where a prime denotes differentiation with respect to η.

10 Characteristic Equation

For $f(\eta) \propto \exp(i\kappa\eta)$, the ordinary-differential equation (41) has the biquadratic characteristic equation

$$\kappa^4 - p\kappa^2 + k = 0. \tag{43}$$

On introducing

$$\gamma = \frac{p}{2\sqrt{k}}, \tag{44}$$

(43) can be written as

$$\kappa^4 - p\kappa^2 + \frac{p^2}{4\gamma^2} = 0. \tag{45}$$

The roots $\pm\kappa_+$ and $\pm\kappa_-$ of (45) are determined by (dimensionless) wavenumbers κ_+ and κ_- defined by

$$\kappa_\pm = \sqrt{\frac{p(\gamma \pm \sqrt{\gamma^2 - 1})}{2\gamma}}. \tag{46}$$

In view of (40), (44), and (46), the dimensionless effective compressive load p and the dimensionless stiffness k of the effective elastic foundation can be expressed in terms of the wavenumbers κ_+ and κ_- by the remarkably simple relations

$$p = \kappa_+^2 + \kappa_-^2 \quad \text{and} \quad k = \kappa_+^2 \kappa_-^2. \tag{47}$$

11 Determination of the Lagrange Multiplier

The definition (44) can be used to express the Lagrange multiplier ε^* in terms of the applied stretch ε and the parameter γ. Toward doing so, note that, by $(34)_{2,3}$ and (40),

$$p = \frac{\varepsilon^* - 2\bar{\varepsilon}}{r^2 \bar{\varepsilon}} \quad \text{and} \quad k = \frac{\varepsilon - \varepsilon^* + \bar{\varepsilon}}{r^4 \bar{\varepsilon}}, \tag{48}$$

where

$$r = \frac{L_1}{L_2} \tag{49}$$

denotes the aspect ratio of the sheet.

As a trivial consequence of (44),

$$\varepsilon^* - 2\bar{\varepsilon} = 2\gamma \sqrt{\bar{\varepsilon}(\varepsilon - \varepsilon^* + \bar{\varepsilon})}. \tag{50}$$

Further, squaring both sides of (50) and solving for ε^* leads to two potential relations,

$$\varepsilon_\pm^* = 2\big(1 \pm \gamma \sqrt{e + \gamma^2} - \gamma^2\big)\bar{\varepsilon}, \tag{51}$$

for ε^*, where

$$e = \frac{\varepsilon - \bar{\varepsilon}}{\bar{\varepsilon}} \tag{52}$$

denotes the relative applied stretch. By (38), $e > 0$ and the roots defined by (51) are both real. Consider $\varepsilon_+^* - 2\bar{\varepsilon}$ and $\varepsilon_-^* - 2\bar{\varepsilon}$. Bearing in mind from (44) that γ is nonnegative, (51) yields

$$\varepsilon_+^* - 2\bar{\varepsilon} = 2\gamma\big(\sqrt{e + \gamma^2} - \gamma\big)\bar{\varepsilon} \geq 2\gamma\big(\gamma - \gamma\big)\bar{\varepsilon} = 0, \tag{53}$$

so that $\varepsilon_+^* \geq 2\bar{\varepsilon} > 0$, and

$$\varepsilon_-^* - 2\bar{\varepsilon} = -2\gamma\big(\sqrt{e + \gamma^2} + \gamma\big)\bar{\varepsilon} < 0, \tag{54}$$

whence $\varepsilon_-^* < 2\bar{\varepsilon}$. By $(34)_2$, $(36)_1$, and $(40)_1$, the difference $\varepsilon^* - 2\bar{\varepsilon}$ must be nonnegative. The root ε_-^* must therefore be discarded and the Lagrange multiplier ε^* must be given in terms of e and γ by

$$\varepsilon^* = 2\big(1 + \gamma \sqrt{e + \gamma^2} - \gamma^2\big)\bar{\varepsilon}. \tag{55}$$

12 Alternative Expressions for the Dimensionless Effective Compressive Load, the Dimensionless Stiffness of the Effective Elastic Foundation, and the Wavenumbers

Having determined the specific form of the Lagrange multiplier ε^*, it is now possible to express the dimensionless effective compressive load p, the dimensionless stiffness k of the effective elastic foundation, and the wavenumbers κ_+ and κ_- in terms of the applied stretch ε and the parameter γ. Specifically, using (55) in $(48)_1$ and $(48)_2$ yields

$$p = \frac{2\gamma(\sqrt{e+\gamma^2}-\gamma)}{r^2} \tag{56}$$

and

$$k = \frac{(\sqrt{e+\gamma^2}-\gamma)^2}{r^4}, \tag{57}$$

respectively. Further, using (56) in (46) yields

$$\kappa_\pm = \frac{1}{r}\sqrt{\big(\sqrt{e+\gamma^2}-\gamma\big)\big(\gamma \pm \sqrt{\gamma^2-1}\big)}. \tag{58}$$

The relations (56) and (57) underscore once again the interdependence, noted previously in the paragraph after (38), between the parameters P and K entering the ordinary-differential equation (32) (or, equivalently, the parameters p and k entering the dimensionless counterpart (41) of (32)). For an actual beam on an elastic foundation with dimensionless stiffness k subject to a dimensionless compressive axial load p, the parameters p and k can be varied independently and $\gamma = p/2\sqrt{k}$ is simply an auxiliary parameter. However, for the problem under consideration here, p and k both depend on the relative applied stretch $e = (\varepsilon - \bar{\varepsilon})/\bar{\varepsilon}$ and γ must be determined through (44) for each relevant value of e.

Solving (56) for $\sqrt{e+\gamma^2}$, squaring both sides of the resulting equation, using the definition (44) of γ yields a simple relation,

$$e = r^2(p + r^2 k), \tag{59}$$

for the relative applied stretch e in terms of the dimensionless effective compressive load p and the dimensionless stiffness k of the effective elastic foundation. Further, invoking the relations (47) for p and k in terms of the wavenumbers κ_+ and κ_- shows that

$$e = r^2(\kappa_+^2 + \kappa_-^2 + r^2\kappa_+^2\kappa_-^2). \tag{60}$$

Provided that κ_+ and κ_- are real, (60) implies that e is positive and, thus, in view of (52), is consistent with the requirement (38) that, for wrinkling to occur, the applied stretch ε must exceed the threshold $\bar{\varepsilon}$.

13 Solution of the Boundary-Value Problem

Bearing in mind that, by (44), γ is nonnegative, the expressions (46) for the roots $\pm\kappa_+$ and $\pm\kappa_-$ of the characteristic equation (43) indicate the presence of three regimes:

- $0 \le \gamma < 1$,
- $\gamma = 1$,

- $\gamma > 1$.

For $0 \leq \gamma < 1$, κ^+ and κ^- are complex conjugates and solutions to the ordinary-differential equation (41) are exponentially damped sinusoids. For $\gamma = 1$, the κ^+ and κ^- coalesce into a single real root and solutions to the ordinary-differential equation (41) are sinusoids. For $\gamma > 1$, κ^+ and κ^- are real and solutions to the ordinary-differential equation (41) are, as in the case $\gamma = 1$, sinusoids.

The three cases are now considered separately. For this purpose, it is often convenient to work with the scaled wavenumber combinations

$$\xi_+ = \frac{1}{2}\pi(\kappa_+ + \kappa_-) \quad \text{and} \quad \xi_- = \frac{1}{2}\pi(\kappa_+ - \kappa_-), \tag{61}$$

which, by (58), can be expressed in terms of e and γ by

$$\xi_\pm = \frac{\pi}{2r^2}\sqrt{\sqrt{e+\gamma^2}-\gamma}\left(\sqrt{\gamma+\sqrt{\gamma^2-1}} \pm \sqrt{\gamma-\sqrt{\gamma^2-1}}\right). \tag{62}$$

13.1 Exponentially Damped Oscillatory Solutions Are Impossible

Since, for $0 \leq \gamma < 1$, the wavenumbers κ_+ and κ_- are complex conjugates, it follows from (61) that ξ_+ is real and that ξ_- is imaginary. The general solution to the ordinary differential equation (41) therefore admits the representation

$$\begin{aligned} f(\eta) = &\left[\tilde{A}\cos\left(\frac{\xi_+}{\pi}\eta\right) + \tilde{B}\sin\left(\frac{\xi_+}{\pi}\eta\right)\right]\cosh\left(\frac{\xi_-}{\pi}\eta\right) \\ &+ \left[\tilde{C}\cos\left(\frac{\xi_+}{\pi}\eta\right) + \tilde{D}\sin\left(\frac{\xi_+}{\pi}\eta\right)\right]\sinh\left(\frac{\xi_-}{\pi}\eta\right), \end{aligned} \tag{63}$$

where $\tilde{A}$, $\tilde{B}$, $\tilde{C}$, and $\tilde{D}$ are arbitrary amplitudes. To provide a solution to the boundary-value problem (41), (63) must satisfy the boundary conditions (42). These conditions yield a homogeneous system of four linear equations for the amplitudes $\tilde{A}$, $\tilde{B}$, $\tilde{C}$, and $\tilde{D}$. For this system to have a nontrivial solution, its determinant must vanish. This solvability condition takes the form

$$\xi_+^2 \sinh^2\xi_- - \xi_-^2 \sin^2\xi_+ = 0. \tag{64}$$

However, since $\sinh\xi \geq \xi \geq \sin\xi$ for all $\xi \geq 0$, with equality possible only for $\xi = 0$,

$$\xi_+^2 \sinh^2\xi_- - \xi_-^2 \sin^2\xi_+ \geq \xi_-^2\left(\xi_+^2 - \sin^2\xi_+\right) \geq 0. \tag{65}$$

By (62), neither ξ_+ nor ξ_- can vanish unless $\gamma = 1$. However, since $0 \leq \gamma < 1$, it follows from (65) that $\xi_+^2 \sinh^2\xi_- - \xi_-^2 \sin^2\xi_+ > 0$, whereby the condition (64) cannot hold. Hence, the dimensionless boundary-value problem (41)–(42) does not admit exponentially damped oscillatory solutions.

13.2 Oscillatory Solutions with a Single Wavenumber Are Impossible

Since, for $\gamma = 1$, the wavenumbers κ_+ and κ_- coalesce, it follows from (61) that $\xi_+ = \pi\kappa_\pm$ and $\xi_- = 0$. The general solution to the ordinary differential equation (41) therefore admits

the representation

$$f(\eta) = \left(\tilde{A} + \frac{\tilde{B}\xi_+}{\pi}\eta\right)\cos\left(\frac{\xi_+}{\pi}\eta\right) + \left(\tilde{C} + \frac{\tilde{D}\xi_+}{\pi}\eta\right)\sin\left(\frac{\xi_+}{\pi}\eta\right), \tag{66}$$

where, as in the case considered previously, $\tilde{A}$, $\tilde{B}$, $\tilde{C}$, and $\tilde{D}$ are arbitrary amplitudes. To provide a solution to the boundary-value problem (41), (66) must satisfy the boundary conditions (42). These conditions yield a homogeneous system of four linear equations for the amplitudes $\tilde{A}$, $\tilde{B}$, $\tilde{C}$, and $\tilde{D}$. For this system to have a nontrivial solution, its determinant must vanish. This solvability condition can be expressed as

$$\xi_+^2 - \sin^2\xi_+ = 0. \tag{67}$$

Since $\xi \geq \sin\xi$ for all $\xi \geq 0$, with equality possible only for $\xi = 0$, it follows that the solvability condition (67) holds only for $\xi_+ = 0$. In this event, (66) yields the trivial solution $y \equiv 0$. Hence, the dimensionless boundary-value problem (41)–(42) does not admit oscillatory solutions involving a single wavenumber. This rules out solutions of the kind considered by Cerda and Mahadevan [31].

13.3 Oscillatory Solutions with Two Distinct Wavenumbers

Since, for $\gamma > 1$, the wavenumbers κ_+ and κ_- are real, distinct, and, by (58), obey

$$\kappa_+ > \kappa_- > 0, \tag{68}$$

it follows from (61) that

$$\xi_+ > \xi_-, \qquad \xi_+ > 0, \qquad \xi_- > 0. \tag{69}$$

Thus, the general solution of (41) admits the representation

$$\begin{aligned} f(\eta) = &\left[\tilde{A}\cos\left(\frac{\xi_+}{\pi}\eta\right) + \tilde{B}\sin\left(\frac{\xi_+}{\pi}\eta\right)\right]\cos\left(\frac{\xi_-}{\pi}\eta\right) \\ &+ \left[\tilde{C}\cos\left(\frac{\xi_+}{\pi}\eta\right) + \tilde{D}\sin\left(\frac{\xi_+}{\pi}\eta\right)\right]\sin\left(\frac{\xi_-}{\pi}\eta\right), \end{aligned} \tag{70}$$

where, as in both cases considered previously, $\tilde{A}$, $\tilde{B}$, $\tilde{C}$, and $\tilde{D}$ are arbitrary amplitudes. To provide a solution to the boundary-value problem (41), (70) must satisfy the boundary conditions (42). These conditions yield a homogeneous system of four linear equations for the amplitudes $\tilde{A}$, $\tilde{B}$, $\tilde{C}$, and $\tilde{D}$. For this system to have a nontrivial solution, its determinant must vanish. This solvability condition can be expressed as

$$\xi_+^2 \sin^2\xi_- - \xi_-^2 \sin^2\xi_+ = 0. \tag{71}$$

In contrast to what occurs for $0 \leq \gamma < 1$ and $\gamma = 1$, for $\gamma > 1$ there exist nontrivial choices of ξ_+ and ξ_- that satisfy the inequalities (69) and the solvability condition (71). Examples of such choices include, but are not limited to, $\xi_+ = (m+1)\pi$ and $\xi_- = \pi$ for any element m of the set $\mathbb{N} = \{1, 2, \dots\}$ of natural numbers.

13.3.1 Admissible Wavenumber Pairs

In view of (61), the solvability condition (71) is satisfied if and only if the wavenumbers κ_+ and κ_- satisfy either

$$\mathcal{F}^+(\kappa_+,\kappa_-)=\frac{\sin[\frac{1}{2}\pi(\kappa_++\kappa_-)]}{\kappa_++\kappa_-}+\frac{\sin[\frac{1}{2}\pi(\kappa_+-\kappa_-)]}{\kappa_+-\kappa_-}=0 \tag{72}$$

or

$$\mathcal{F}^-(\kappa_+,\kappa_-)=\frac{\sin[\frac{1}{2}\pi(\kappa_++\kappa_-)]}{\kappa_++\kappa_-}-\frac{\sin[\frac{1}{2}\pi(\kappa_+-\kappa_-)]}{\kappa_+-\kappa_-}=0. \tag{73}$$

Any pair (κ_+,κ_-) that is consistent with the inequalities (68) and obeys either (72) or (73) is admissible in the sense that, via (61) and (70), it provides a wrinkled solution of the dimensionless boundary-value problem (41)–(42).

The collection of all admissible wavenumber pairs forms a countably infinite collection of curves in the lower half of the first quadrant of the (κ_+,κ_-)-plane. In particular, for each natural number m, the strip

$$\mathcal{S}_m=\{(\kappa_+,\kappa_-):\kappa_+-(2m-1)>\kappa_->\kappa_+-(2m+1),\kappa_+>\kappa_->0\} \tag{74}$$

contains exactly one curve

$$\mathcal{C}_m^+=\{(\kappa_+,\kappa_-)\in\mathcal{S}_m:\mathcal{F}^+(\kappa_+,\kappa_-)=0\} \tag{75}$$

determined by (72) and exactly one curve

$$\mathcal{C}_m^-=\{(\kappa_+,\kappa_-)\in\mathcal{S}_m:\mathcal{F}^-(\kappa_+,\kappa_-)=0\} \tag{76}$$

determined by (73). The curves $\mathcal{C}_m^+$ and $\mathcal{C}_m^-$ emanate from the line $\kappa_-=0$ at $\kappa_+=2m$ and $\kappa_+=2\zeta_m$, respectively, where ζ_m is the m-th positive root of $\tan(\pi\zeta)=\pi\zeta$ and, as is readily demonstrated, obeys

$$\zeta_m>m. \tag{77}$$

Due to the periodic properties of $\mathcal{F}^+$ and $\mathcal{F}^-$, the curves $\mathcal{C}_m^+$ and $\mathcal{C}_m^-$ intersect at each point in the set

$$\mathcal{I}_m=\{(\kappa_+,\kappa_-):\kappa_+=2m+n,\kappa_-=n,n\in\mathbb{N}\}. \tag{78}$$

A continuity argument shows that $\mathcal{C}_m^+$ is above $\mathcal{C}_m^-$ up to the first point of $\mathcal{I}_m$, below $\mathcal{C}_m^-$ between the first and second points of $\mathcal{I}_m$, above $\mathcal{C}_m^-$ between the second and third points of $\mathcal{I}_m$, and so on ad infinitum. A plot depicting portions of the curves $\mathcal{C}_m^\pm$, for $m=1,2,3$, appears in Fig. 1.

13.3.2 Functional Relations Between the Dimensionless Effective Compressive Load and the Relative Applied Stretch

For the classical problem of the buckling of a beam on an elastic foundation, the collections of ordered pairs (κ_+,κ_-) comprising the curves $\mathcal{C}_m^+$ and $\mathcal{C}_m^-$ are used parametrically in the relations $(47)_1$ and $(47)_2$ for p and k through κ_+ and κ_- to construct plots of $\sqrt{k}$ versus p (Hetényi [41]). When performed for each natural number m, this construction reveals

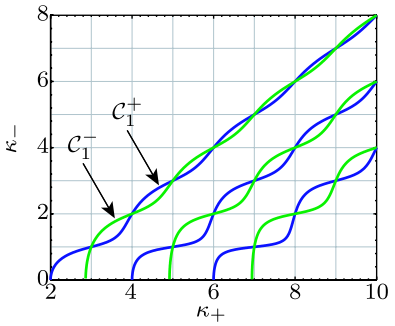

Fig. 1 Plot depicting portions of the curves $\mathcal{C}_m^{\pm}$ for $m = 1, 2, 3$, with $\mathcal{C}_1^+$ and $\mathcal{C}_1^-$ indicated specifically

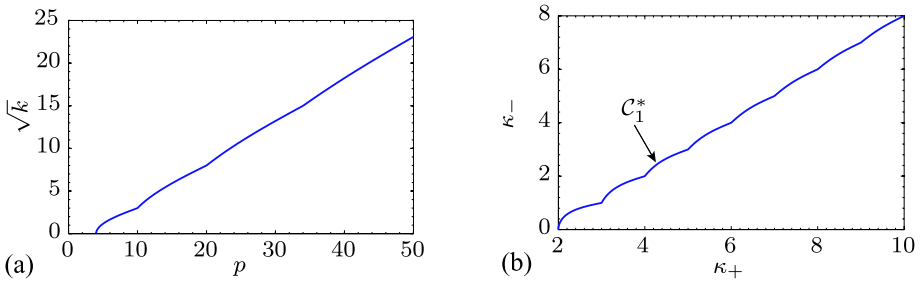

Fig. 2 (**a**) Plot of the square root $\sqrt{k}$ of the dimensionless effective foundational stiffness k versus the least critical dimensionless effective compressive load p as determined in the classical buckling problem. (**b**) Collection of ordered pairs (κ_+, κ_-) belonging to the upper envelope $\mathcal{C}_1^*$ of $\mathcal{C}_1^{\pm}$

a multiplicity of values of p for each choice of k. The choice is then made to select the minimum value of p for each k—thereby providing the least critical buckling load for a given foundational stiffness. The corresponding plot of $\sqrt{k}$ versus p (Fig. 2a) is determined parametrically by using the collection of ordered pairs (κ_+, κ_-) belonging to the piecewise smooth upper envelope

$$\mathcal{C}_1^* = \max_{\kappa_-} \left\{ (\kappa_+, \kappa_-) : \frac{\sin[\frac{1}{2}\pi(\kappa_+ + \kappa_-)]}{\kappa_+ + \kappa_-} \pm \frac{\sin[\frac{1}{2}\pi(\kappa_+ - \kappa_-)]}{\kappa_+ - \kappa_-} = 0 \right\} \tag{79}$$

of $\mathcal{C}_1^{\pm}$ (Fig. 2b). For future reference, let

$$\mathcal{A} = \{(\kappa_+, \kappa_-) : \kappa_+ = n + 2, \kappa_- = n, n \in \mathbb{N} \cup \{0\}\} \tag{80}$$

denote the set of points formed by the starting point of $\mathcal{C}_1^*$ and all points where the tangent to $\mathcal{C}_1^*$ is discontinuous.[5]

For the wrinkling problem, the physically relevant control parameter is the relative applied stretch e (or, equivalently, the applied stretch $\varepsilon = (1 + e)\bar{\varepsilon}$) and, in contrast to the classical buckling problem, p and k are merely auxiliary measures of the effective compressive loading and the foundational stiffness that are induced by stretching of the sheet. In view of the relations $(47)_1$ and (60) determining p and e through κ_+ and κ_-, a parametric

[5] In view of (78), $\mathcal{A} = \{(2, 0)\} \cup \mathcal{I}_1$.

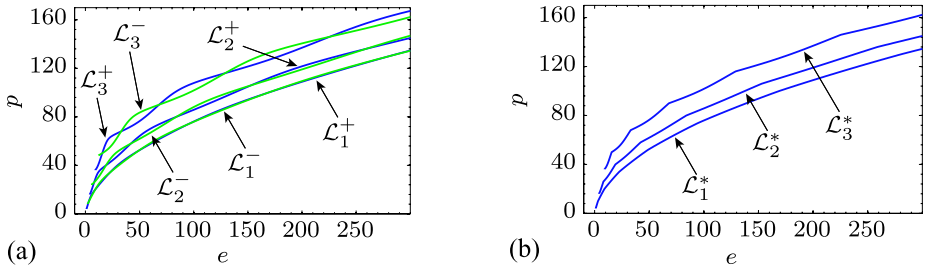

Fig. 3 (**a**) Plots of the curves $\mathcal{L}_1^{\pm}$, $\mathcal{L}_2^{\pm}$, and $\mathcal{L}_3^{\pm}$ determining the dimensionless effective compressive load p as a function of the relative applied stretch e parametrically through the ordered pairs (κ_+, κ_-) defining the curves $\mathcal{C}_1^{\pm}$, $\mathcal{C}_2^{\pm}$, and $\mathcal{C}_3^{\pm}$. (**b**) Plots of the lower envelopes $\mathcal{L}_1^*$, $\mathcal{L}_2^*$, and $\mathcal{L}_3^*$ of $\mathcal{L}_1^{\pm}$, $\mathcal{L}_2^{\pm}$, and $\mathcal{L}_3^{\pm}$

construction analogous to that used in the classical buckling problem can be used to yield plots of p versus e; plots of k versus e can then be obtained using (59). This process reveals that $\mathcal{C}_m^+$ and $\mathcal{C}_m^-$ have strictly increasing images $\mathcal{L}_m^+$ and $\mathcal{L}_m^-$ in the first quadrant of the (e, p)-plane. Moreover, since $\mathcal{C}_m^+$ and $\mathcal{C}_m^-$ intersect at each point in $\mathcal{I}_m$, it follows from $(47)_1$ and (60) that $\mathcal{L}_m^+$ and $\mathcal{L}_m^-$ intersect at each point in

$$\mathcal{J}_m = \{(e, p) : e = e_n^m, p = p_n^m, n \in \mathbb{N}\}, \tag{81}$$

where e_n^m and p_n^m are defined by

$$e_n^m = r^2((2m+n)^2(1+r^2n^2)+n^2) \tag{82}$$

and

$$p_n^m = (2m+n)^2 + n^2. \tag{83}$$

Moreover, in view of (77), a continuity argument leads to the conclusion that $\mathcal{L}_m^+$ is below $\mathcal{L}_m^-$ up to the first point of $\mathcal{J}_m$, above $\mathcal{L}_m^-$ between the first and second points of $\mathcal{J}_m$, below $\mathcal{L}_m^-$ between the second and third points of $\mathcal{J}_m$, and so on ad infinitum. Plots depicting portions of the curves $\mathcal{L}_1^{\pm}$, $\mathcal{L}_2^{\pm}$, and $\mathcal{L}_3^{\pm}$, appear in Fig. 3a.

Simple considerations show that, for any value of the relative applied stretch e greater than or equal to $4r^2\zeta_m^2$, there exist at least $2m$ distinct values of the dimensionless effective compressive load p. This absence of uniqueness is closely analogous to what occurs in the classical problem of the buckling of a beam on an elastic foundation. Motivated by the approach taken in the classical problem, it seems reasonable to choose the least possible value of p associated to each possible value of e. The values of e and p corresponding to this choice belong to the lower envelope $\mathcal{L}_1^*$ of $\mathcal{L}_1^{\pm}$. The curve $\mathcal{L}_1^*$ can be constructed parametrically by using the values of κ_+ and κ_- on the curve $\mathcal{C}_1^*$ in $(47)_1$ and (60). The collection of physically observable wavenumbers for the wrinkling problem is therefore identical to that arising in the classical buckling problem. Plots depicting $\mathcal{L}_1^*$ along with the next two lower envelopes $\mathcal{L}_2^*$ of $\mathcal{L}_2^{\pm}$ and $\mathcal{L}_3^*$ of $\mathcal{L}_3^{\pm}$ appear in Fig. 3b.

Plots of the minimum dimensionless compressive load p versus e, for aspect ratios $r = 5/3$, $r = 2$, and $r = 5/2$, appear in Fig. 4a. The trend demonstrates that, for a given value e of the relative applied stretch, the value p of the effective dimensionless compressive load required to induce wrinkling increases as the aspect ratio $r = L_1/L_2$ decreases. Thus, the greater L_2 is with respect to L_1, the greater is the effective compressive load required to induce wrinkling. Figure 4b shows that plotting p versus e/r^4 leads to a collapse of the

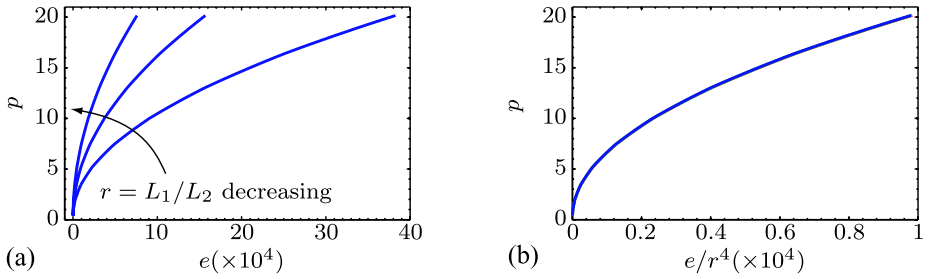

Fig. 4 (**a**) Plots of the minimum dimensionless effective compressive load p versus e for aspect ratios $r = L_1/L_2$ of 5/3, 2, and 5/2. (**b**) The p versus e curves collapse to a single curve when p is plotted versus e/r^4

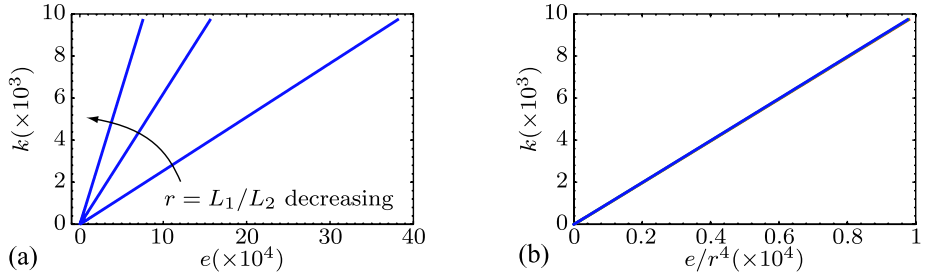

Fig. 5 (**a**) Plots of the dimensionless stiffness k of the effective elastic foundation versus e for aspect ratios $r = L_1/L_2$ of 5/3, 2, and 5/2. (**b**) The k versus e curves collapse to a single curve when k is plotted versus e/r^4

curves in Fig. 4a onto a single curve. Serrations, although not evident in Fig. 4a, are present in the p versus e relations for all values of r; consistent with this observation, magnification of Fig. 4b also reveals serrations. Plots of the dimensionless stiffness k of the effective elastic foundation versus e, as determined by (59) with knowledge of e and p, for aspect ratios $r = 5/3$, $r = 2$, and $r = 5/2$, appear in Fig. 5a. Except for values of e close to r^2, the relation between k and e is linear. The trend shows that, for a given value of e of the relative applied stretch, the value k of the dimensionless stiffness of the effective elastic foundation required to induce wrinkling increases as $r = L_1/L_2$ decreases. The stiffness of the effective elastic foundation therefore behaves analogously to the effective compressive load. Figure 5b shows that plotting k versus e/r^4 leads to a collapse of the curves in Fig. 5a onto a single curve.

Using the (48) and (52) in (44) produces an expression for γ in terms of e. Plots of γ^{-1} versus $e^{1/4}$ appear in Fig. 6a for $r = 5/3$, $r = 2$, and $r = 5/2$. These plots show that γ decreases with $r = L_1/L_2$. Moreover, regardless of the value of r, γ decreases with e and, consistent with the restriction $\gamma > 1$, obeys

$$\inf_{e\to\infty} \gamma = 1.$$

Figure 6b shows that, but for low values of the abscissa, plotting γ^{-1} versus $e^{1/4}/r$ leads to a collapse of curves in Fig. 6a onto a single curve.

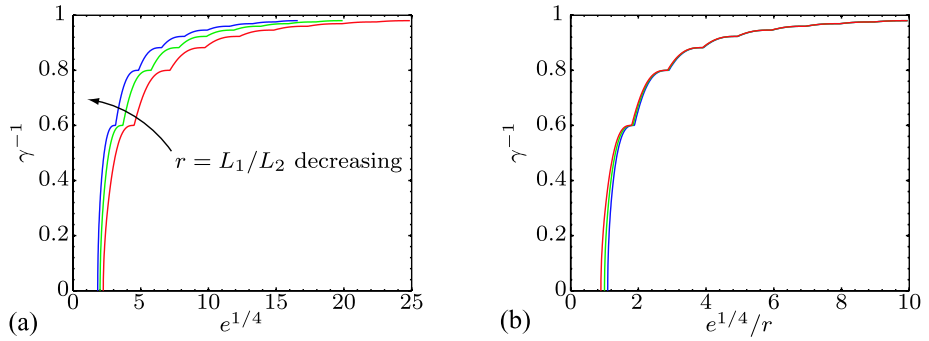

Fig. 6 (**a**) Plots of $\gamma^{-1} = 2\sqrt{k}/p$ versus $e^{1/4}$ for aspect ratios $r = L_1/L_2$ of 5/3, 2, and 5/2. (**b**) The curves collapse to a single curve when γ^{-1} is plotted versus $e^{1/4}/r$

13.3.3 Characterization of Wrinkled Solutions

Granted a general solution f of the form (70) to the ordinary-differential equation (41), the boundary conditions (42) give rise to a homogeneous linear system of equations for the amplitudes $\tilde{A}$, $\tilde{B}$, $\tilde{C}$, and $\tilde{D}$. The rank of the coefficient matrix of that system is equal to either two or three depending upon whether both (72) and (73) hold or only one of (72) and (73) holds. Hence, the coefficient matrix is of rank two only at the countably infinite set of wavenumber pairs $\mathcal{I}_1$ defined in (78). Elsewhere along the curve $\mathcal{C}_1^*$, three of the four amplitudes in (70) can be determined. Hereafter, attention is therefore restricted to the solution set $\mathcal{C}_1^* \setminus \mathcal{I}_1$. Knowledge of solutions modulo an unknown amplitude is sufficient to characterize the shape of f and to compute the number of wrinkles. To this end, it is convenient to express f in the alternative, but equivalent, form

$$f(\eta) = \hat{A}\cos(\kappa_-\eta) + \hat{B}\sin(\kappa_-\eta) + \hat{C}\sin(\kappa_+\eta) + \hat{D}\cos(\kappa_+\eta), \tag{84}$$

with

$$\tilde{A} = \hat{A} + \hat{D}, \qquad \tilde{D} = \hat{A} - \hat{D}, \qquad \tilde{B} = \hat{B} + \hat{C}, \qquad \tilde{C} = \hat{C} - \hat{B}, \tag{85}$$

and to rearrange the boundary conditions (42) so that the corresponding coefficient matrix is block diagonal. Specifically, the conditions

$$f'\left(\frac{\pi}{2}\right) = f'\left(-\frac{\pi}{2}\right) \quad \text{and} \quad f''\left(\frac{\pi}{2}\right) = -f''\left(-\frac{\pi}{2}\right) \tag{86}$$

involve only $\hat{A}$ and $\hat{D}$, while only $\hat{B}$ and $\hat{C}$ appear in

$$f'\left(\frac{\pi}{2}\right) = -f'\left(-\frac{\pi}{2}\right) \quad \text{and} \quad f''\left(\frac{\pi}{2}\right) = f''\left(-\frac{\pi}{2}\right). \tag{87}$$

Whereas (86) and (87) are implied, separately, by (42), these conditions must be combined to ensure satisfaction of (42).

When (73) holds, so that $\mathcal{F}^-(\kappa_+, \kappa_-) = 0$, (86) are linearly dependent and

$$\hat{A} = \alpha\hat{D}, \quad \text{with } \alpha = -\frac{\kappa_+ \sin(\frac{1}{2}\pi\kappa_+)}{\kappa_- \sin(\frac{1}{2}\pi\kappa_-)} \quad \text{or} \quad \alpha = -\frac{\kappa_+^2 \cos(\frac{1}{2}\pi\kappa_+)}{\kappa_-^2 \cos(\frac{1}{2}\pi\kappa_-)}. \tag{88}$$

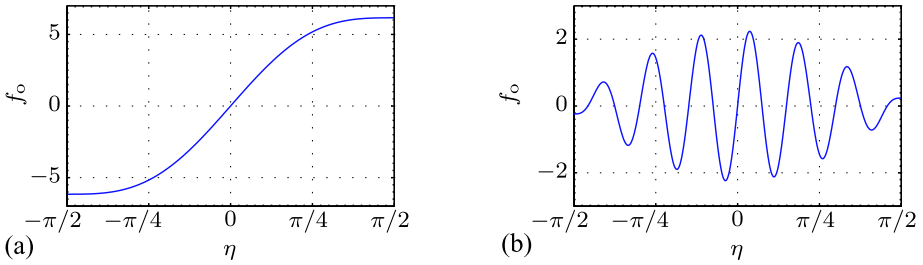

Fig. 7 Plot of wrinkle profile $f_o(\eta) = \beta \sin(\kappa_- \eta) + \sin(\kappa_+ \eta)$. (**a**) $\kappa_+ = 2.5$, $\kappa_- = 0.8$, $\beta = 7.21$. (**b**) $\kappa_+ = 14.5$, $\kappa_- = 12.5$, $\beta = 1.25$

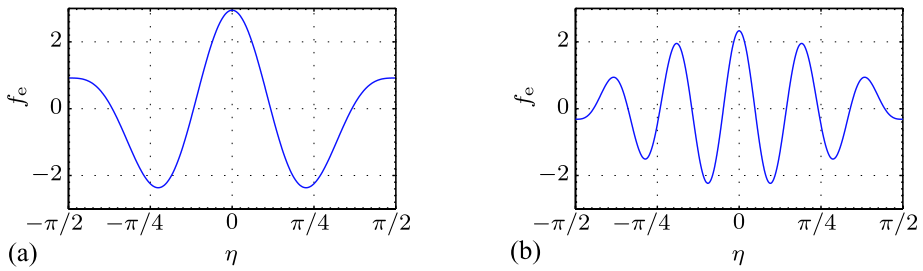

Fig. 8 Plot of wrinkle profile $f_e(\eta) = \alpha \cos(\kappa_- \eta) + \cos(\kappa_+ \eta)$. (**a**) $\kappa_+ = 5.5$, $\kappa_- = 3.63$, $\alpha = 1.95$. (**b**) $\kappa_+ = 11.5$, $\kappa_- = 9.56$, $\alpha = 1.33$

Hence, $\mathcal{C}_1^-$ characterizes wrinkled states that are symmetric about the line $\eta = 0$ (that is, bearing in mind $(39)_1$, about the line $x_2 = 0$). Alternatively, when (72) holds, so that $\mathcal{F}^+(\kappa_+, \kappa_-) = 0$, equations (87) are linearly dependent and

$$\hat{B} = \beta \hat{C}, \quad \text{with } \beta = -\frac{\kappa_+ \cos(\frac{1}{2}\pi\kappa_+)}{\kappa_- \cos(\frac{1}{2}\pi\kappa_-)} \quad \text{or} \quad \beta = -\frac{\kappa_+^2 \sin(\frac{1}{2}\pi\kappa_+)}{\kappa_-^2 \sin(\frac{1}{2}\pi\kappa_-)}. \tag{89}$$

Hence, $\mathcal{C}_1^+$ characterizes wrinkled states that are odd about the line $\eta = 0$ (that is, bearing in mind $(39)_1$, about the line $x_2 = 0$). In summary, f can be rewritten as

$$f(\eta) = \begin{cases} \hat{C} f_o(\eta) & \text{for } (\kappa_+, \kappa_-) \text{ in } \mathcal{C}_1^+ \setminus \mathcal{I}_1, \\ \hat{D} f_e(\eta) & \text{for } (\kappa_+, \kappa_-) \text{ in } \mathcal{C}_1^- \setminus \mathcal{I}_1, \end{cases} \tag{90}$$

where odd function f_o and even function f_e defined by

$$f_o(\eta) = \beta \sin(\kappa_- \eta) + \sin(\kappa_+ \eta) \quad \text{and} \quad f_e(\eta) = \alpha \cos(\kappa_- \eta) + \cos(\kappa_+ \eta), \tag{91}$$

are linear combinations of two sinusoids.

Plots of f_o, for $\kappa_+ = 2.50$, $\kappa_- = 0.80$, and $\beta = 7.21$ and for $\kappa_+ = 14.5$, $\kappa_- = 12.5$, and $\beta = 1.25$ are displayed in Fig. 7, while plots of f_e, for $\kappa_+ = 5.50$, $\kappa_- = 3.63$, $\alpha = 1.95$ and for $\kappa_+ = 11.5$, $\kappa_- = 9.56$, $\alpha = 1.33$ are in displayed Fig. 8. For increasing values of κ_+, the number of wrinkles increases and a sinusoidal envelope enclosing the wrinkles, as depicted in Figs. 7b and 8b, approaches wavelength 2π. The wrinkle amplitude therefore decays toward the free edges (that is, toward $x_2 = \pm L_2$). With reference to (61) and (70),

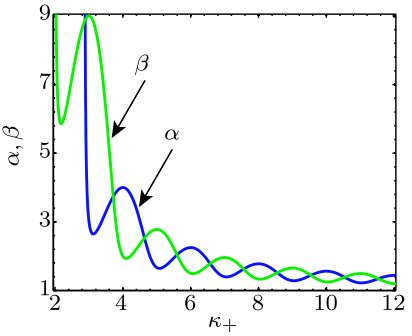

Fig. 9 Plots of α and β versus κ_+ along the curves $\mathcal{C}_1^-$ and $\mathcal{C}_1^+$ respectively

the wrinkles are associated with the wavenumber ξ_+/π while the envelope is associated with the wavenumber ξ_-/π. If the relation $\kappa_+ = \kappa_- + 2$ is substituted into (61), ξ_-/π reduces to unity. This relation is exactly valid for (κ_+, κ_-) in set $\mathcal{I}_1$, as is evident from (78), and is well approximated for large values of κ_+ along curves $\mathcal{C}_1^+$ and $\mathcal{C}_1^-$, as depicted in Fig. 1. Further insight concerning the envelope can be obtained from Fig. 9, where α along $\mathcal{C}_1^-$ and β along $\mathcal{C}_1^+$ are plotted versus κ_+. Evidently, for large values of κ_+, α and β both approach unity from above. When this occurs, $(85)_2$, $(85)_4$, (88) and (89) imply that $\tilde{D}$ and $\tilde{C}$ tend to 0 and (70) reduces to

$$f(\eta) = \begin{cases} 2\hat{C}\sin\left(\dfrac{\xi_+}{\pi}\eta\right)\cos\left(\dfrac{\xi_-}{\pi}\eta\right) & \text{for } (\kappa_+, \kappa_-) \text{ in } \mathcal{C}_1^+ \setminus \mathcal{I}_1, \\ 2\hat{D}\cos\left(\dfrac{\xi_+}{\pi}\eta\right)\cos\left(\dfrac{\xi_-}{\pi}\eta\right) & \text{for } (\kappa_+, \kappa_-) \text{ in } \mathcal{C}_1^- \setminus \mathcal{I}_1, \end{cases} \tag{92}$$

consistent with previous discussion of the limit shape of the envelope $\cos(\xi_-/\pi\,\eta)$ and the roles of ξ_+/π and ξ_-/π.

There is some latitude in defining the number of wrinkles. For future reference let

$$W = \left\{\eta_i, i = 1, 2 \ldots n_w : |\eta_i| \le \frac{\pi}{2},\, f'(\eta_i) = 0\right\}, \tag{93}$$

be the collection of roots of f'. Their number is $n_w = n + 2$. Two of them occur at the edges and correspond to $\eta = \pm\pi/2$, while the remaining n lie between $-\pi/2$ and $\pi/2$. Here, the number of wrinkles is identified with n_w—i.e. with the number of extrema of f. In view of this convention, the number n_w of wrinkles in Figs. 7a ($\kappa_+ = 2.5$), 8a ($\kappa_+ = 5.5$), 8b ($\kappa_+ = 11.5$), and 7b ($\kappa_+ = 14.5$) is respectively equal to 2, 5, 11, and 14.

While continuously increasing κ_+ or κ_-, the number of wrinkles changes suddenly. Consider the curve $\mathcal{C}_1^+$. In view of (90) and (91), the corresponding solution f_o, is odd and it follows that n_w is even. Whenever ξ_+/π attains an even value, two new wrinkles appear. In particular, for

$$n \le \frac{\xi_+}{\pi} < n + 2, \quad \text{or} \quad n + 1 \le \kappa_+ < n + 3, \tag{94}$$

with n even in $\mathbb{N} \cup \{0\}$, there are exactly $n + 2$ wrinkles. For future convenience, inequality (94) is stated equivalently also in terms of κ_+ using the relation $\xi_+/\pi = \kappa_+ - 1$ which is obtained from (61) and (78) and holds on set $\mathcal{I}_1$, where ξ_+/π and κ_+ are integers. An analogous result holds for $\mathcal{C}_1^-$ and f_e. The number of wrinkles is in this case odd and for $n \le \xi_+/\pi < n + 2$ or $n + 1 \le \kappa_+ < n + 3$ with n odd, there are $n + 2$ wrinkles.

Consider now $\mathcal{C}_1^*$ and Figs. 1 and 2b. For $n+1 \le \kappa_+ < n+2$, $n \in \mathbb{N}$, $\mathcal{C}_1^+$ belongs to the lower envelope of $\mathcal{C}_1^+$ and $\mathcal{C}_1^-$. On the other hand, $\mathcal{C}_1^+$ belongs to the upper envelope $\mathcal{C}_1^*$ when

$$n+2 \le \kappa_+ < n+3, \tag{95}$$

holds with n even in $\mathbb{N} \cup \{0\}$, $n+2$ being also the number of wrinkles. Similarly, $\mathcal{C}_1^-$ belongs to the upper envelope $\mathcal{C}_1^*$ and has $n+2$ wrinkles when (95) holds with n odd. Summarizing, for the actual solution curve $\mathcal{C}_1^*$ there are $n_w = n+2$ wrinkles when (95) is satisfied. When κ_+ reaches one of the integer values in $\mathcal{I}_1$, the number of wrinkles increases by unity. The number of wrinkles n_w can alternatively be expressed in terms of κ_+ as

$$n_w = \lfloor \kappa_+ \rfloor = \max\{m \in \mathbb{N}, m \le \kappa_+\}. \tag{96}$$

13.3.4 Critical Values of the Applied Stretch, the Effective Compressive Load, and the Stiffness of the Effective Elastic Foundation

The collection of wavenumber pairs belonging to the set $\mathcal{A}$ defined in (80) can be used to determine sequences of critical values of the applied stretch ε, the effective compressive load P, and the stiffness K of the effective elastic foundation.

Specifically, by (35), (49), (52), and (60), the sequence of critical values of the applied stretch is $\{\varepsilon_n, n \in \mathbb{N} \cup \{0\}\}$, with

$$\varepsilon_n = \frac{\pi^2 h^2}{48(1-\nu^2)L_1^2}\left[1 + \frac{L_1^2}{L_2^2}\left((n+2)^2\left(1 + \frac{L_1^2 n^2}{L_2^2}\right) + n^2\right)\right]. \tag{97}$$

Similarly, by $(34)_1$, (40), and (47), the associated sequences of the effective compressive load and the stiffness of the effective elastic foundation are $\{P_n, n \in \mathbb{N}\}$ and $\{K_n, n \in \mathbb{N}\}$, with

$$P_n = \frac{\pi^2 E h^3}{24(1-\nu^2)L_2^2}(n^2+2n+2) \quad \text{and} \quad K_n = \frac{\pi^4 E h^3}{192(1-\nu^2)L_2^4} n^2 (n+2)^2. \tag{98}$$

With regard to (97), it is possible to obtain the asymptotic values of ε_n when the aspect ratio r is much smaller or much larger than unity: when the sheet is much longer than it is wide, so that $L_1 \gg L_2$, ε_n is approximated by

$$\varepsilon_n \approx \frac{\pi^2 h^2}{48(1-\nu^2)L_1^2}\left(\frac{L_1^4}{L_2^4} n^2 (n+2)^2\right); \tag{99}$$

when the sheet is much wider than it is long, so that $L_1 \ll L_2$, ε_n is approximated by

$$\varepsilon_n \approx \frac{\pi^2 h^2}{48(1-\nu^2)L_1^2}\left(1 + \frac{L_1^2}{L_2^2}(2n^2+4n+4)\right). \tag{100}$$

Interestingly for large values of r, $\varepsilon_n \sim r^4 n^4$, while for small values of r, $\varepsilon_n \sim r^2 n^2$. Thus, it is easier to induce n wrinkles in a sheet that is considerably wider than it is long: with respect to a sheet that is longer than it is wide, the hindrance of the Poisson contraction at the clamped edges is more pronounced. Moreover, a greater width allows more room to geometrically accommodate wrinkles.

In view of (35) and (52), the applied stretch necessary to induce wrinkling must exceed the critical value

$$\varepsilon_0 = \frac{\pi^2 h^2}{48(1-\nu^2)L_1^2}\left(1+4\frac{L_1^2}{L_2^2}\right). \tag{101}$$

The necessary condition (38) therefore underestimates the threshold value of applied stretch by a factor of $1+4L_1^2/L_2^2$. The applied stretch that must be exceeded to induce bifurcation to a wrinkled state therefore increases as the length $2L_1$ of the specimen increases with respect to the height $2L_2$ of the specimen. By (98), the critical effective compressive load P_0 generated by the critical applied stretch ε_0 is

$$P_0 = \frac{\pi^2 E h^3}{12(1-\nu^2)L_2^2}. \tag{102}$$

Incidentally, this value corresponds to the compressive critical load for the buckling of wide plates; there, the factor $1/(1-\nu^2)$ represents a stiffening against anticlastic bending. Further, by $(98)_2$, the critical stiffness K_0 of the effective elastic foundation generated by the critical applied stretch ε_0 vanishes. For bifurcation to a wrinkled state to occur, P and K must exceed P_0 and $K_0 = 0$, respectively.

Let n be in $\mathbb{N}\cup\{0\}$. Then, for any value of the applied stretch ε in the interval $(\varepsilon_n, \varepsilon_{n+1})$, (61) and (70) provide a solution to the dimensionless boundary-value problem (41)–(42) with $n+2$ wrinkles. The values of the effective compressive load P and the stiffness K of the effective elastic foundation that accompany such a solution must lie in the intervals (P_n, P_{n+1}) and (K_n, K_{n+1}).

Although the critical applied stretch ε_n corresponding to the onset of bifurcation to a state with $n+2$ wrinkles depends on the length, width, and thickness of the sheet, the corresponding values P_n and K_n of the effective compressive load and stiffness of the effective elastic foundation depend on the width and thickness but not on the length of the sheet.

14 Determination of the Amplitudes and Wavelengths

14.1 Determination of the Amplitudes

In Sect. 13.3.3, knowledge of the solution f to the boundary-value problem (41)–(42), modulo an unknown coefficient, was exploited to describe the shape of the cross-width wrinkle profiles and to compute the number of wrinkles. Here, the unknown coefficient entering f in (90) is determined by imposing the linearization of the geometric constraint (20).

The wrinkle amplitude is not constant along the length $2L_1$ of the sheet. The Ansatz (31) assumes that the deflection w achieves a maximum at the midlength $x_1 = 0$ and vanishes at the clamped edges $x_1 = \pm L_1$. In what follows, the wrinkle amplitude is evaluated at $x_1 = 0$. With this provision, using (31) and (39), the relationship between w and f at $x_1 = 0$ is simply

$$w(0, x_2) = y(x_2) = 2L_2 f(\eta). \tag{103}$$

The analysis of (41)–(42) carried out in Sect. 13 reveals that the wrinkle amplitude is not constant across the width $2L_2$ either. Instead, the wrinkle amplitude decays toward the free edges $\eta = \pm\pi/2$ (that is, by $(39)_1$, toward $x_2 = \pm L_2$).

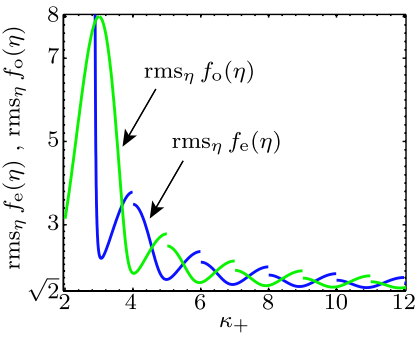

Fig. 10 Plots of $\mathrm{rms}_\eta\, f_\mathrm{e}(\eta)$ and $\mathrm{rms}_\eta\, f_\mathrm{o}(\eta)$ versus κ_+ along curves $\mathcal{C}_1^-$ and $\mathcal{C}_1^+$ respectively

In what follows, two alternative characterizations of the overall wrinkle amplitude are provided. First, to facilitate comparisons with the work of Cerda, Ravi-Chandar and Mahadevan [30], the root-mean-square value of the wrinkle amplitudes is determined. Second, to facilitate a comparison with as yet unavailable measurements, the maximum value of the wrinkle amplitude is determined. The maximum wrinkle amplitude is presumably easier to determine experimentally and less affected by measurement errors than would be the root-mean-square amplitude.

14.1.1 Root-Mean-Square of Wrinkle Amplitude

In view of the definition (93) of the set W of the roots η_i of the first derivative of f and the assumption that the wrinkle amplitude is evaluated at $x_1 = 0$, the root-mean-square of the wrinkle amplitude is given by

$$A_\mathrm{rms} = 2L_2 \operatorname*{rms}_\eta f(\eta), \tag{104}$$

where, recalling that W has cardinality n_w, $\mathrm{rms}_\eta\, f(\eta)$ is defined by

$$\operatorname*{rms}_\eta f(\eta) = \sqrt{\frac{\sum_{\eta_i \in W} f^2(\eta_i)}{n_w}}. \tag{105}$$

Thus, by (90),

$$A_\mathrm{rms} = \begin{cases} 2L_2|\hat{D}| \operatorname*{rms}_\eta f_\mathrm{e}(\eta) & \text{for } (\kappa_+, \kappa_-) \in \mathcal{C}_1^- \setminus \mathcal{I}_1, \\ 2L_2|\hat{C}| \operatorname*{rms}_\eta f_\mathrm{o}(\eta) & \text{for } (\kappa_+, \kappa_-) \in \mathcal{C}_1^+ \setminus \mathcal{I}_1, \end{cases} \tag{106}$$

where $|\hat{D}|$ and $|\hat{C}|$ are determined by imposing the linearization of the geometric constraint (20).

Figure 10 provides plots of $\mathrm{rms}_\eta\, f_\mathrm{e}(\eta)$ along $\mathcal{C}_1^-$ and of $\mathrm{rms}_\eta\, f_\mathrm{o}(\eta)$ along $\mathcal{C}_1^+$ versus κ_+. Evidently, for large values of κ_+,

$$\operatorname*{rms}_\eta f_\mathrm{e}(\eta) \to \sqrt{2} \quad \text{and} \quad \operatorname*{rms}_\eta f_\mathrm{o}(\eta) \to \sqrt{2}. \tag{107}$$

Each jump in Fig. 10 corresponds to an increase by two of the number of wrinkles in the solution as discussed in the paragraph containing (94). As a result of the "new" wrinkles, the denominator in (105) increases abruptly, thus producing the observed drop in the root-mean-square value. These discontinuities in the root-mean-square computed along curves $\mathcal{C}_1^+$ and

$\mathcal{C}_1^-$ should not be confused with the serrations in curve $\mathcal{C}_1^*$ which are due to the switch of the solution from curve $\mathcal{C}_1^+$ to $\mathcal{C}_1^-$ and vice versa as visible in Figs. 1 and 2b.

When linearized in accord with the small slope approximation (28), the geometric constraint (20) reads

$$\frac{1}{8L_1L_2}\int_{-L_1}^{L_1}\int_{-L_2}^{L_2}(w_{,1}^2+w_{,2}^2)\,\mathrm{d}x_2\,\mathrm{d}x_1=\varepsilon g(v,\varepsilon). \tag{108}$$

In view of (31), (39), and (49), the linearized constraint (108) simplifies to

$$\frac{\pi}{4}\int_{-\frac{\pi}{2}}^{\frac{\pi}{2}}\left(\frac{f^2(\eta)}{r^2}+(f'(\eta))^2\right)\mathrm{d}\eta=\varepsilon g(v,\varepsilon). \tag{109}$$

On substituting (84) into the integral on the left side of (109), it follows that

$$\begin{aligned}&\int_{-\frac{\pi}{2}}^{\frac{\pi}{2}}\left(\frac{f^2(\eta)}{r^2}+(f'(\eta))^2\right)\mathrm{d}\eta\\&\quad=\frac{\pi}{2}(a_+\beta^2+2b_+\beta+c_+)\hat{C}^2+\frac{\pi}{2}(a_-\alpha^2+2b_-\alpha+c_-)\hat{D}^2,\end{aligned} \tag{110}$$

where $a_\pm$, $b_\pm$, and $c_\pm$ are defined by

$$\left.\begin{aligned}a_\pm&=\left(\kappa_-^2+\frac{1}{r^2}\right)\pm\left(\kappa_-^2-\frac{1}{r^2}\right)\operatorname{sinc}(\pi\kappa_-),\\b_\pm&=\left(\kappa_+\kappa_-+\frac{1}{r^2}\right)\operatorname{sinc}\left[\frac{1}{2}\pi(\kappa_+-\kappa_-)\right]\\&\quad\pm\left(\kappa_+\kappa_--\frac{1}{r^2}\right)\operatorname{sinc}\left[\frac{1}{2}\pi(\kappa_++\kappa_-)\right],\\c_\pm&=\left(\kappa_+^2+\frac{1}{r^2}\right)\pm\left(\kappa_+^2-\frac{1}{r^2}\right)\operatorname{sinc}(\pi\kappa_+),\end{aligned}\right\} \tag{111}$$

with

$$\operatorname{sinc}x=\begin{cases}1 & \text{if } x=0\\ \dfrac{\sin x}{x} & \text{if } x\neq 0.\end{cases}$$

With reference to (111), as κ_+ and κ_- increase along $\mathcal{C}_1^*$, terms originating from $w_{,1}^2$, which are proportional to r^{-2}, become negligible with respect to terms due to $w_{,2}^2$, which are quadratic in κ_+ and κ_-. Thus, at least for sufficiently large κ_+ and κ_-, the left side of (108) is well-approximated by the linearization of the constraint (19) imposed by Cerda and Mahadevan [31].

Next, since, by (110),

$$|\hat{D}|=\frac{2\sqrt{2}}{\pi}\sqrt{\frac{\varepsilon g(v,\varepsilon)}{a_-\alpha^2+2b_-\alpha+c_-}}\quad\text{on}\quad\mathcal{F}^- \tag{112}$$

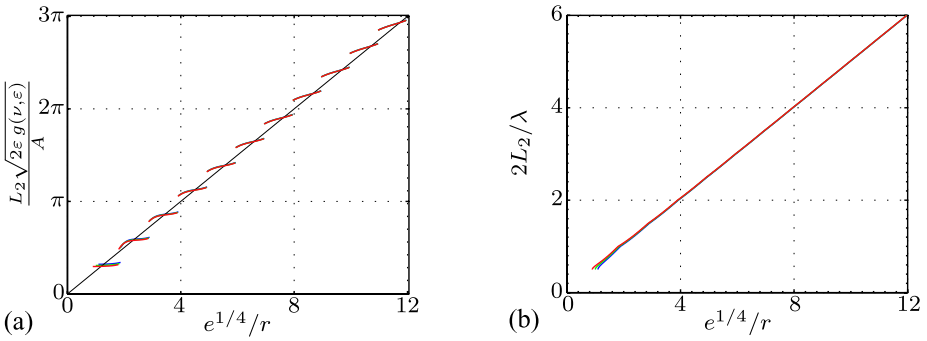

Fig. 11 (**a**) The inverse $1/A_{\rm rms}$ of the root-mean-square of the wrinkle amplitude, multiplied by $L_2\sqrt{2\varepsilon\, g(\nu,\varepsilon)}$, versus $e^{1/4}/r$ plotted for r equal 5/3, 2, and 5/2. The *straight continuous line* indicates the linear trend and, for $g(\nu,\varepsilon)=\nu$, coincides with the result of Cerda and Mahadevan [31]. (**b**) The inverse of wrinkle wavelength $2L_2/\lambda$ versus $e^{1/4}/r$ plotted for r equal 5/3, 2, and 5/2

and

$$|\hat{C}| = \frac{2\sqrt{2}}{\pi}\sqrt{\frac{\varepsilon g(\nu,\varepsilon)}{a_+\beta^2+2b_+\beta+c_+}} \quad \text{on} \quad \mathcal{F}^+, \tag{113}$$

(106) can be used to determine the wrinkle amplitude $A_{\rm rms}$. The result is depicted in Fig. 11a, where the inverse $1/A_{\rm rms}$ of the root-mean-square amplitude, multiplied by $L_2\sqrt{2\varepsilon\, g(\nu,\varepsilon)}$, is plotted against $e^{1/4}/r$ for three representative values of r. The plot shows that, except for very low values of the abscissa, the distinct curves collapse onto a single curve with a linear trend of slope $\pi/4$ represented by a thin continuous line. As explained in forthcoming Sect. 15.2, provided that g is chosen so that $g(\nu,\varepsilon)=\nu$, this line coincides with the scaling relation for the amplitude obtained by Cerda and Mahadevan [31]. The jumps in the plot correspond to the points of solution set $\mathcal{I}_1$ where the amplitude cannot be computed. At each point in $\mathcal{I}_1$, the number of wrinkles increases by unity and the solution changes abruptly from symmetric to antisymmetric or vice versa about the line $\eta=0$ (that is, bearing in mind $(39)_1$, about the line $x_2=0$).

14.1.2 Maximum Amplitude

By analogy to the definition (104) of the root-mean-square amplitude $A_{\rm rms}$, the maximum amplitude $A_{\rm max}$ is defined as

$$A_{\rm max} = 2L_2 \max_{\eta} |f(\eta)| \tag{114}$$

and is computed via (90)

$$A_{\rm max} = \begin{cases} 2L_2|\hat{D}|\ \max_\eta\ f_{\rm e}(\eta) & \text{for } (\kappa_+,\kappa_-)\in \mathcal{C}_1^-\setminus\mathcal{I}_1, \\ 2L_2|\hat{C}|\ \max_\eta\ f_{\rm o}(\eta) & \text{for } (\kappa_+,\kappa_-)\in \mathcal{C}_1^+\setminus\mathcal{I}_1. \end{cases} \tag{115}$$

The maximum values of $f_{\rm e}$ and $f_{\rm o}$ are displayed in Fig. 12 for increasing κ_+. It is seen that

$$\lim_{\kappa_+\to\infty}\left(\max_\eta f_{\rm e}(\eta)\right) = \lim_{\kappa_+\to\infty}\left(\max_\eta f_{\rm o}(\eta)\right) = 2. \tag{116}$$

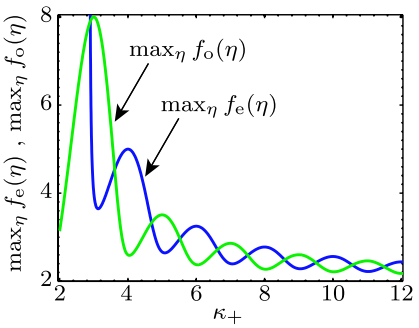

Fig. 12 Plots of $\max_\eta f_e(\eta)$ and $\max_\eta f_o(\eta)$ versus κ_+ along curves $\mathcal{C}_1^-$ and $\mathcal{C}_1^+$ respectively

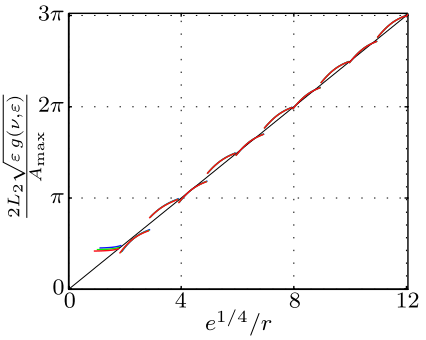

Fig. 13 The inverse $1/A_{\max}$ of the maximum amplitude, multiplied by $2L_2\sqrt{\varepsilon\, g(\nu,\varepsilon)}$, plotted versus $e^{1/4}/r$ for r equal 5/3, 2, and 5/2. The *black line* indicates the linear trend

On substituting (112) and (113) into (115) and using the computed values of $\max_\eta f_e(\eta)$ and $\max_\eta f_o(\eta)$, the maximum amplitude is obtained. The inverse, $1/A_{\max}$, of that amplitude, multiplied by $2L_2\sqrt{\varepsilon\, g(\nu,\varepsilon)}$, is plotted versus $e^{1/4}/r$ in Fig. 13 for r equal 5/3, 2, and 5/2. Again, different values of the aspect ratio r affect the amplitude only for low values of the abscissa, but, with respect to Fig. 11a, the deviation from the linear trend, indicated by a thin continuous line, is less significant.

14.2 Determination of the Wavelengths

The general solution (70) of the ordinary differential equation (41) is characterized by two distinct wavenumbers ξ_+/π and ξ_-/π. The former and larger of these is associated with wrinkles. Consistent with this observation, and bearing in mind $(39)_1$, the wavelength λ of wrinkles is here defined as

$$\lambda = 2L_2\frac{2\pi}{\xi_+} = \frac{4\pi L_2}{\xi_+}. \tag{117}$$

In Fig. 11b, the inverse $1/\lambda$ of the wavelength, multiplied by $2L_2$, is plotted against $e^{1/4}/r$ for three representative values of r. As with the root-mean-square and maximum wrinkle amplitudes, except for very low values of the abscissa, the distinct curves collapse onto a single straight line, in this case with slope 1/2, which is easily deduced either graphically and analytically.

Regarding the remaining wavenumber ξ_-/π, as κ_+ and κ_- increase along $\mathcal{C}_1^*$, ξ_-/π rapidly converges to unity, while the associated wavelength tends to $4L_2$. As shown in Figs. 7b and 8b and discussed in the paragraph between (91) and (93), this indicates that

the wrinkle profile is enclosed within an envelope of half-sine shape that attains its maximum at $\eta = 0$ (that is, at $x_2 = 0$) and vanishes at the edges (that is, at $x_2 = \pm L_2$).

15 Scaling Relations

Scaling relations for the wavelength λ and the root-mean-square and maximum amplitudes $A_{\rm rms}$ and $A_{\rm max}$ are now sought in terms of the geometric and material properties of the sheet. These scaling relations are based on the assumption that the applied stretch ε is large compared to $\bar{\varepsilon}$ as defined by (35), viz.

$$\varepsilon \gg \bar{\varepsilon}, \tag{118}$$

so that, by (52)

$$e \gg 1 \quad \text{and} \quad e \approx \varepsilon/\bar{\varepsilon}. \tag{119}$$

The primary goal of this exercise is to compare the scaling relations predicted by the theory developed here with the analogous predictions

$$\lambda_{\rm CM} = \sqrt[4]{\frac{16\pi^2 h^2 L_1^2}{3(1-\nu^2)\varepsilon}} \quad \text{and} \quad A_{\rm CM} = \sqrt[4]{\frac{64 h^2 L_1^2 \nu^2 \varepsilon}{3\pi^2(1-\nu^2)}} \tag{120}$$

obtained by Cerda and Mahadevan [31].

15.1 Wavelength

Granted (119), (60) and (61) imply that

$$\kappa_\pm \approx \frac{e^{1/4}}{r} \quad \text{and} \quad \xi_+ \approx \frac{\pi e^{1/4}}{r}. \tag{121}$$

Using (121) and recalling the expressions (35) and (49) for $\bar{\varepsilon}$ and r in the definition (117) of the wrinkle wavelength λ yields the estimate

$$\lambda \approx \frac{4L_2 r}{e^{1/4}} = \sqrt[4]{\frac{16\pi^2 h^2 L_1^2}{3(1-\nu^2)\varepsilon}} = \lambda_{\rm CM}. \tag{122}$$

Hence, provided that ε is sufficiently large compared to $\bar{\varepsilon}$, the scaling relation for the wavelength predicted by the theory developed here is identical to that predicted by Cerda and Mahadevan [31]. Moreover, (122) agrees both with Fig. 11b and with the experimental measurements of Cerda, Ravi-Chandar and Mahadevan [30].

Remarkably (122) agrees quantitatively also with the scaling relation obtained by Wong and Pellegrino in [33] for the wavelength of wrinkles in a sheared thin sheet. The comparison of course holds under the provision that the length of the wrinkles and the maximum principal strain are aptly translated to that different setting.

15.2 Root-Mean-Square of Wrinkle Amplitude

Regarding the amplitude, bearing in mind Fig. 9, the definitions (88) and (89) of α and β yield

$$\alpha \approx 1, \quad \text{and} \quad \beta \approx 1, \tag{123}$$

while the definitions $(91)_1$ and $(91)_2$ of f_e and f_o give

$$\operatorname*{rms}_{\eta} f_e(\eta) \approx \sqrt{2}, \quad \text{and} \quad \operatorname*{rms}_{\eta} f_o(\eta) \approx \sqrt{2}. \tag{124}$$

Next, since, by (111) and (123),

$$\lim_{e\to+\infty} (a_-\alpha^2 + 2b_-\alpha + c_-) \to 2\kappa_\pm^2 \tag{125}$$

and

$$\lim_{e\to+\infty} (a_+\beta^2 + 2b_+\beta + c_+) \to 2\kappa_\pm^2, \tag{126}$$

the expressions (112) and (113) for $\hat{D}$ and $\hat{C}$ yield

$$\hat{C} \approx \frac{2r}{\pi e^{1/4}}\sqrt{\varepsilon g(\nu,\varepsilon)} \quad \text{and} \quad \hat{D} \approx \frac{2r}{\pi e^{1/4}}\sqrt{\varepsilon g(\nu,\varepsilon)}. \tag{127}$$

Using (123), (124) and (127) and the expressions (35) and (49) for $\bar{\varepsilon}$ and r in the (106) for the wrinkle amplitude A_{rms} generates the estimate

$$A_{\text{rms}} \approx \left(2L_2\frac{2r}{\pi e^{1/4}}\sqrt{\varepsilon g(\nu,\varepsilon)}\right)\sqrt{2} \approx \frac{4\sqrt{2}}{\pi}L_1\sqrt[4]{\varepsilon\bar{\varepsilon}}\sqrt{g(\nu,\varepsilon)}$$

$$= \sqrt{g(\nu,\varepsilon)}\sqrt[4]{\frac{64h^2L_1^2\varepsilon}{3\pi^2(1-\nu^2)}} = \sqrt{\frac{g(\nu,\varepsilon)}{\nu}}A_{\text{CM}}. \tag{128}$$

The scaling relation (128) matches the slope graphically deduced from Fig. 11a and, if g is chosen to obey $g(\nu,\varepsilon) = \nu$, coincides with a result obtained by Cerda and Mahadevan [31]. However, (128) allows, through the presence of the factor $\sqrt{g(\nu,\varepsilon)}$, which appears on the right side of the geometric constraint (20), for different scaling dependencies of the wrinkle amplitude on Poisson's ratio ν and the applied stretch ε. Moreover, there is a significant difference between the structure of the wrinkled states described by the theory developed here and those postulated by Cerda and Mahadevan [31]. Here, the wrinkle amplitude decays from the center length $x_2 = 0$ toward the free edges $x_2 = \pm L_2$ of the specimen. In contrast, Cerda and Mahadevan [31] consider only wrinkled states in which the wrinkle amplitude is uniform from edge to edge of the specimen.

Comparison with the scaling relation for the amplitude of wrinkles obtain by Wong and Pellegrino in [33] for a sheared thin sheet shows (128) coincides quantitatively with their result provided that g is chosen so that $g(\nu,\varepsilon) = (1-\nu)/2$. It is interesting to observe that, for $\nu = 1/3$, $\nu = (1-\nu)/2 = 1/3$ and the choices of $g(\nu,\varepsilon) = \nu$ and $g(\nu,\varepsilon) = (1-\nu)/2$ coincide. Furthermore, in the experiments of Cerda, Ravi-Chandar and Mahadevan [30] and of Wong and Pellegrino [34], the value of ν is near 1/3—0.35 for Cerda, Ravi-Chandar and Mahadevan and 0.31 for Wong and Pellegrino. These observations suggest that accurate measurements of the amplitudes and further tests might be needed to single out the appropriate choice of the quantity g entering the constraint and ascertain the actual through-width wrinkle profile.

15.3 Maximum Amplitude

An analogous scaling relationship can be obtained for the maximum wrinkle amplitude $A_{\max}$ by simply replacing (124) with

$$\max_{\eta} f_{\mathrm{e}}(\eta) \approx 2, \quad \text{and} \quad \max_{\eta} f_{\mathrm{o}}(\eta) \approx 2, \tag{129}$$

whence it follows that

$$A_{\max} \approx \left(2L_2\sqrt{\varepsilon g(\nu,\varepsilon)}\right)\frac{4}{\pi}\frac{r}{e^{1/4}} = \sqrt{2}A_{\mathrm{rms}} = \sqrt{2}\sqrt{\frac{g(\nu,\varepsilon)}{\nu}}A_{\mathrm{CM}}, \tag{130}$$

which coincides with the linear trend drawn in Fig. 13. It is not surprising that $A_{\max} \approx \sqrt{2}A_{\mathrm{rms}}$ since it is well known that the quadratic mean of a sinusoid is $\sqrt{2}$ times smaller than its maximum value and all extrema of f lie approximately on a sinusoidal envelope of wavenumber ξ_-/π.

15.4 Number of Wrinkles

As noted in (96), the number n_w of wrinkles coincides with the integer part $\lfloor \kappa_+ \rfloor$ of κ_+. Equation (60) is now used to determine a scaling relation for n_w. Granted (118) and (119), the values of κ_+ and κ_- are sufficiently large to ensure that

$$\kappa_+ \approx \kappa_- + 2 \quad \text{and} \quad \kappa_+^2 + \kappa_-^2 \ll \kappa_+^2\kappa_-^2. \tag{131}$$

In particular, $(131)_1$ holds exactly for all points in set $\mathcal{I}_1$ determined by setting $m = 1$ in (78). It therefore follows that

$$n_w \approx \left\lfloor \sqrt{\sqrt{\frac{e}{r^4}} + 1} \right\rfloor + 1,$$

which, using again (119), yields the scaling

$$n_w \approx \left\lfloor \frac{e^{1/4}}{r} \right\rfloor + 1 \approx \left\lfloor 2L_2\sqrt[4]{\frac{3\varepsilon(1-\nu^2)}{\pi^2 h^2 L_1^2}} \right\rfloor + 1. \tag{132}$$

A comparison of (132) with the analogous result (122) for the wavelength λ reveals that

$$n_w \approx \lfloor 4L_2/\lambda \rfloor + 1. \tag{133}$$

As expected, the number of wrinkles is therefore inversely proportional to the wavelength. Moreover, whereas, by (122), the wavelength λ does not depend explicitly on L_2, n_w is directly proportional to L_2.

15.5 Range of Validity of the Estimates

To assess the validity range of the assumption (119) made at the beginning of this section, consider a polyethylene sheet with dimensions and properties identical to that used in the experiments of Cerda, Ravi-Chandar, and Mahadevan [30]: $h = 0.01$ cm, $L_1 = 10$ cm,

$\nu = 0.35$. Then, by (35), $\bar{\varepsilon} = 2.34 \times 10^{-7}$. This seems to suggest an almost global validity for the scaling relationship. Consistent with this observation, Fig. 11b shows that the most significant deviation between the estimate (122) and the actual expression for λ, though essentially negligible, occurs for very small values of $e^{1/4}/r$. Similar conclusions arise from considering Figs. 11a and 13, the second of which indicates that the estimate (130) for the maximum amplitude $A_{\max}$ deviates most markedly from the actual expression for $A_{\max}$ when e obeys $e^{1/4} < 2r$, or, equivalently, by (35), (49), and (52), whenever ε obeys

$$\varepsilon < \left(1 + 16\frac{L_1^4}{L_2^4}\right)\frac{\pi^2 h^2}{48(1-\nu^2)L_1^2}. \tag{134}$$

Thus, since, by (97),

$$\varepsilon_0 < \left(1 + 16\frac{L_1^4}{L_2^4}\right)\frac{\pi^2 h^2}{48(1-\nu^2)L_1^2} < \varepsilon_2, \tag{135}$$

values of ε that exceed ε_0 but satisfy (134) generate states involving at most three wrinkles. Thus, the scaling relations (120), (122), (128), and (130) apply whenever more than three wrinkles are present.

16 Concluding Remarks

The formulation and subsequent analysis described here show that for a rectangular sheet of length $2L_1$, width $2L_2$, and thickness h, with Young's modulus E and Poisson's ratio ν, gripped on the edges $x_1 = \pm L_1$ and subjected to a stretch ε:

1. There is a sequence $\{\varepsilon_n, n \in \mathbb{N} \cup \{0\}\}$ of critical applied stretches, with

$$\varepsilon_n = \frac{\pi^2 h^2}{48(1-\nu^2)L_1^2}\left[1 + \frac{L_1^2}{L_2^2}\left((n+2)^2\left(1 + \frac{L_1^2 n^2}{L_2^2}\right) + n^2\right)\right],$$

   at which abrupt configuration changes take place. For $\varepsilon_n \le \varepsilon < \varepsilon_{n+1}$, the sheet possesses $n+2$ wrinkles. As the aspect ratio L_1/L_2 decreases, the stretch ε_n required to induce $n+2$ wrinkles in a sheet also decreases because the effect of the gripped edges hindering the Poisson contraction is felt more and the relatively larger width allows for more room to geometrically accommodate wrinkles. In particular, for large values of the aspect ratio L_1/L_2, ε_n scales with the fourth power of L_1/L_2, while, for small values of L_1/L_2, ε_n scales with the square of the same argument.
2. When ε is equal to or greater than ε_0, so that wrinkling occurs, the sheet adopts a wrinkled profile characterized by wavenumbers κ_+ and κ_- belonging to the locus

$$\max_{\kappa_-}\left\{(\kappa_+, \kappa_-) : \frac{\sin[\frac{1}{2}\pi(\kappa_+ + \kappa_-)]}{\kappa_+ + \kappa_-} \pm \frac{\sin[\frac{1}{2}\pi(\kappa_+ - \kappa_-)]}{\kappa_+ - \kappa_-} = 0\right\}.$$

   Whereas $\xi_+ = \frac{1}{2}\pi(\kappa_+ + \kappa_-)$ characterizes the number of wrinkles, $\xi_- = \frac{1}{2}\pi(\kappa_+ - \kappa_-)$, which is close to π, envelopes the wrinkle profile in a half-wave that determines its coarse shape.

3. Whenever ε exceeds ε_2 and, thus, is sufficiently large to induce four or more wrinkles, the wavelength λ and amplitude A_{rms} of the wrinkled profile admit the estimates

$$\lambda \approx \sqrt[4]{\frac{16\pi^2 h^2 L_1^2}{3(1-\nu^2)\varepsilon}} \quad \text{and} \quad A_{\text{rms}} \approx \sqrt{g(\nu,\varepsilon)}\sqrt[4]{\frac{64h^2 L_1^2 \varepsilon}{3\pi^2(1-\nu^2)}},$$

the first of which coincides with the scaling relation for wavelength obtained by Cerda, Ravi-Chandar and Mahadevan [30] and Cerda and Mahadevan [31] and the second of which differs from the scaling relation for amplitude obtained by Cerda, Ravi-Chandar and Mahadevan [30] and Cerda and Mahadevan [31] by a multiplicative factor of $\sqrt{g(\nu,\varepsilon)}$ due to the more general geometric constraint applied here. Importantly, the additional freedom associated with the dependence of g on ν and ε influences only the way in which the amplitude scales with ν and ε but not with the geometry (that is, the thickness and aspect ratio) of the sheet.

The richness of predictions and the concurrent lack of data for critical stretches and wrinkle amplitudes point to the need for further experimental validation.

Acknowledgement The authors thank Reza Loftalian for his thoughtful and accurate remarks concerning an earlier draft of this paper. Financial support from the Canada Research Chairs Program is gratefully acknowledged.

References

1. Blandino, J.D., Johnson, J., Dharamsi, U.K.: Corner wrinkling of a square membrane due to symmetric mechanical loads. J. Spacecr. Rockets **39**, 717–724 (2002)
2. Jenkins, C.H., Kalanovic, V.D., Padmanabhan, K., Faisal, S.M.: Intelligent shape control for precision membrane antennae and reflectors in space. Smart Mater. Struct. **8**, 857–867 (1999)
3. Sakamoto, H., Park, K.C., Miyazaki, Y.: Evaluation of membrane structure designs using boundary web cables for uniform tensioning. Acta Astronaut. **60**, 846–857 (2007)
4. Hudson, D.A., Renshaw, A.: An algorithm for the release of burn contractures of the extremities. Burns **32**, 663–668 (2006)
5. Lott-Crumpler, D.A., Chaudhry, H.R.: Optimal patterns for suturing wounds of complex shapes to foster healing. J. Biomech. **34**, 51–58 (2001)
6. Georgeu, G.A., Ross, D.: Wounds and scars. Surgery **20**, 139–141 (2002)
7. Cerda, E.: Mechanics of scars. J. Biomech. **38**, 1598–1603 (2005)
8. Hofer, S.O.P., Mureau, M.A.M.: Improving outcomes in aesthetic facial reconstruction. Clin. Plast. Surg. **36**, 345–354 (2009)
9. Ueda, K., Hara, M., Okada, M., Kurokawa, N., Otani, K., Nuri, T.: Lambda incision for effective tissue expansion. J. Plast. Reconstr. Aesthet. Surg. doi:10.1016/j.bjps.2009.09.015 (2009)
10. Stafford, C.M., Harrison, C., Beers, K.L., Karim, A., Amis, E.J., Vanlandingham, M.R., Kim, H.-C., Volksen, W., Miller, R.D., Simonyi, E.: A buckling-based metrology for measuring the elastic moduli of polymeric thin films. Nat. Mater. **3**, 545–550 (2004)
11. Chung, J.Y., Chastek, T.Q., Fasolka, M.J., Ro, H.W., Stafford, C.M.: Quantifying residual stress in nanoscale thin polymer films via surface wrinkling. ACS Nano **3**, 844–852 (2009)
12. Burton, K., Taylor, D.L.: Traction forces of cytokinesis measured with optically modified elastic substrata. Nature **385**, 450–454 (1997)
13. Harris, A.K., Wild, P., Stopak, D.: Silicone rubber substrata: a new wrinkle in the study of cell locomotion. Science **208**, 177–179 (1980)
14. Kolaric, B., Vandeparre, H., Desprez, S., Vallee, R.A.L., Damman, P.: In situ tuning the optical properties of a cavity by wrinkling. Appl. Phys. Lett. **96**, 043119 (2010)
15. Ohzono, T., Monobe, H., Shiokawa, K., Fujiwara, M., Shimizu, Y.: Shaping liquid on a micrometre scale using microwrinkles as deformable open channel capillaries. Soft Matter **5**, 4658–4664 (2009)
16. Wagner, H.: Ebene Blechwandträger mit sehr dünnen Stegblechen. ZFM, Z. Flugtech. Mot.luftschiffahrt **20**, 200–207, 227–233, 256–262, 279–284, 306–314 (1929)

17. Wagner, H., Ballerstedt, W.: Über Zugfelder in ursprünglich gekrümmten, dünnen Blechen bei Beanspruchung durch Schubkräfte. Luftfahrtforschung **12**, 70–74 (1935)
18. Wagner, H.: Ëiniges über schalenförmige Flugzeug-Bauteile. Luftfahrtforschung **13**, 281–292 (1936)
19. Kondo, K.: The general solution of the flat tension field. J. Soc. Aeronaut. Sci. Nippon **5**, 887–901 (1938)
20. Reissner, E.: On tension field theory. In: Proceedings of the 5th International Congress for Applied Mechanics, pp. 88–92 (1938)
21. Mansfield, E.H.: Load transfer via a wrinkled membrane. Proc. R. Soc. Lond. Ser. A, Math. Phys. Sci. **316**, 269–289 (1970)
22. Danielson, D.A., Natarajan, S.: Tension field theory and the stress in stretched skin. J. Biomech. **8**, 135–142 (1975)
23. Wu, C.H.: Nonlinear wrinkling of nonlinear membranes of revolution. J. Appl. Mech. **45**, 533–538 (1978)
24. Zak, M.: Statics of wrinkling films. J. Elast. **12**, 51–63 (1982)
25. Pipkin, A.C.: Continuously distributed wrinkles in fabrics. Arch. Ration. Mech. Anal. **95**, 93–115 (1986)
26. Steigmann, D.J., Pipkin, A.C.: Wrinkling of pressurized membranes. J. Appl. Mech. **56**, 624–628 (1989)
27. Steigmann, D.J.: Tension-field theory. Proc. R. Soc. Lond. Ser. A, Math. Phys. Sci. **429**, 141–173 (1990)
28. Hilgers, M.G., Pipkin, A.C.: Elastic sheets with bending stiffness. Q. J. Mech. Appl. Math. **45**, 57–75 (1992)
29. Steigmann, D.J.: Two-dimensional models for the combined bending and stretching of plates and shells based on three-dimensional linear elasticity. Int. J. Eng. Sci. **46**, 654–676 (2008)
30. Cerda, E., Ravi-Chandar, K., Mahadevan, L.: Thin films: Wrinkling of an elastic sheet under tension. Nature **419**, 579–580 (2002)
31. Cerda, E., Mahadevan, L.: Geometry and physics of wrinkling. Phys. Rev. Lett. **90**, 1–4 (2003)
32. Coman, C.: On the applicability of tension field theory to a wrinkling instability problem. Acta Mech. **190**, 57–72 (2007)
33. Wong, Y.W., Pellegrino, S.: Wrinkled membranes II: Analytical models. J. Mech. Mater. Struct. **1**, 27–61 (2006)
34. Wong, Y.W., Pellegrino, S.: Wrinkled membranes I: Experiments. J. Mech. Mater. Struct. **1**, 3–25 (2006)
35. Wong, Y.W., Pellegrino, S.: Wrinkled membranes III: Numerical simulations. J. Mech. Mater. Struct. **1**, 63–95 (2006)
36. Balmforth, N.J., Craster, R.V., Slim, A.C.: On the buckling of elastic plates. Q. J. Mech. Appl. Math. **61**, 267–289 (2008)
37. Landau, L.D., Lifschitz, E.M.: Theory of Elasticity. Pergamon, New York (1970)
38. Bazant, Z.P., Cedolin, L.: Stability of Structures Elastic, Inelastic, Fracture, and Damage Theories. Dover, New York (2003)
39. Podio-Guidugli, P.: A primer in elasticity. J. Elast. **58**, 1–104 (2000)
40. Pipkin, A.C.: Constraints in linearly elastic materials. J. Elast. **6**, 179–193 (1976)
41. Hetényi, M.: Beams on Elastic Foundation. University of Michigan Press, Ann Arbor (1946)